

Shared subcortical arousal systems across sensory modalities during transient modulation of attention

Aya Khalaf^a, Erick Lopez^a, Jian Li^{b,c}, Andreas Horn^{b,d,e,f}, Brian L. Edlow^{b,c}, Hal Blumenfeld^{a,g,h,*}

^a Department of Neurology, Yale University School of Medicine, New Haven, CT, USA

^b Department of Neurology, Center for Neurotechnology and Neurorecovery, Massachusetts General Hospital and Harvard Medical School, Boston, MA, USA

^c Athinoula A. Martinos Center for Biomedical Imaging, Massachusetts General Hospital and Harvard Medical School, Charlestown, MA, USA

^d Department of Neurology, Center for Brain Circuit Therapeutics, Brigham & Women's Hospital and Harvard Medical School, Boston, MA, USA

^e Department of Neurosurgery, Massachusetts General Hospital and Harvard Medical School, Boston, MA, USA

^f Movement Disorders & Neuromodulation Section, Department of Neurology, Charité – Universitätsmedizin, Berlin, Germany

^g Department of Neuroscience, Yale University School of Medicine, New Haven, CT, USA

^h Department of Neurosurgery, Yale University School of Medicine, New Haven, CT, USA

ARTICLE INFO

Key words:

Attention modulation

Arousal

Consciousness

Subcortical networks

fMRI

ABSTRACT

Subcortical arousal systems are known to play a key role in controlling sustained changes in attention and conscious awareness. Recent studies indicate that these systems have a major influence on short-term dynamic modulation of visual attention, but their role across sensory modalities is not fully understood. In this study, we investigated shared subcortical arousal systems across sensory modalities during transient changes in attention using block and event-related fMRI paradigms. We analyzed massive publicly available fMRI datasets collected while 1561 participants performed visual, auditory, tactile, and taste perception tasks. Our analyses revealed a shared circuit of subcortical arousal systems exhibiting early transient increases in activity in midbrain reticular formation and central thalamus across perceptual modalities, as well as less consistent increases in pons, hypothalamus, basal forebrain, and basal ganglia. Identifying these networks is critical for understanding mechanisms of normal attention and consciousness and may help facilitate subcortical targeting for therapeutic neuromodulation.

Introduction

Different sensory modalities elicit distinct neural signatures in the brain. However, it can be proposed that there is a fundamental subset of circuits shared across modalities, supporting core functions such as conscious perception and attention control. Subcortical arousal systems are known to play a key role in controlling sustained changes of attention and long-lasting states such as sleep/wake and levels of vigilance (Steriade and McCarley, 2010). Previous studies on patients with disorders of consciousness confirmed the critical influence of subcortical arousal systems in maintaining states of consciousness (Edlow et al., 2012; Schiff, 2008; Schiff and Plum, 2000). However, the role of these subcortical systems in dynamic modulation of attention has been less studied and when examined, the focus has often been on a single sensory modality without considering the shared networks dynamically

modulating attention across perceptual modalities (Sarter and Lustig, 2020; R Li et al., 2021; Kronemer et al., 2022). Moreover, most research investigating dynamic changes in attention has focused on cortical large-scale networks involved in top-down attentional salience and bottom-up attention control with little emphasis on subcortical systems (Barry et al., 2012; Corbetta and Shulman, 2002; V. V Menon and Uddin, 2010; Seeley et al., 2007).

Subcortical systems have been increasingly recognized as playing an important role in cognition (Janacsek et al., 2022). Studies on healthy participants and patients with impaired consciousness have demonstrated that the midbrain reticular formation and central thalamus are key subcortical structures that modulate attention (Edlow et al., 2012; Schiff, 2008; Schiff and Plum, 2000; R Li et al., 2019; Nagai et al., 2004; Setzer et al., 2022; Van der Werf et al., 2002; Yanaka et al., 2010). Additionally, deep brain stimulation studies in humans and animal

* Corresponding author at: Yale Depts. Neurology, Neuroscience, Neurosurgery 333 Cedar Street, New Haven, CT 06520-8018, USA

E-mail address: hal.blumenfeld@yale.edu (H. Blumenfeld).

<https://doi.org/10.1016/j.neuroimage.2025.121224>

Received 3 February 2025; Received in revised form 15 April 2025; Accepted 15 April 2025

Available online 16 April 2025

1053-8119/© 2025 The Authors. Published by Elsevier Inc. This is an open access article under the CC BY-NC license (<http://creativecommons.org/licenses/by-nc/4.0/>).

models demonstrated that stimulation of the central thalamus significantly improves arousal and restores consciousness (Arnts et al., 2024; Redinbaugh et al., 2020; ND ND Schiff et al., 2007; Tasserie et al., 2022; Xu et al., 2020). Previous research suggests that arousal systems in the thalamus, upper brainstem and basal forebrain may contribute to dynamic modulation of attention and conscious perception (Sarter and Lustig, 2020; R Li et al., 2021; Schiff et al., 2013; Raver and Lin, 2015; Kinomura et al., 1996; Kronemer et al., 2022). The dynamic modulation of attention by the subcortical arousal systems is a key mechanism that facilitates conscious perception. Previously, we introduced a data-driven model that describes the sequence of neural mechanisms required to produce conscious awareness of sensory events (Blumenfeld, 2023). The model hypothesizes that one of the mechanisms critical for conscious perception is an attention mechanism that operates through cortical and subcortical arousal systems, mediating stimulus detection, dynamic modulation of arousal, bottom-up attentional salience, and top-down attentional control. In this framework, the subcortical arousal networks provide an early dynamic transient pulse that facilitates subsequent widespread signals necessary for conscious perception (Blumenfeld, 2023). While multiple cortical systems have been implicated in sensory detection, attention and conscious perception (Corbetta and Shulman, 2002; Kwon et al., 2021; Bollimunta et al., 2018; Koch et al., 2016; Dehaene, 2014; Dosenbach et al., 2008; V V Menon and Uddin, 2010), the potential key role of subcortical arousal networks in modulating attention and perception across sensory modalities requires further investigation.

Functional magnetic resonance imaging (fMRI) experiments typically use block designs, event-related designs, or a combination of both to identify and characterize both sustained and transient blood-oxygenation level-dependent (BOLD) responses (Buckner et al., 1996; Visscher et al., 2003; NU Dosenbach et al., 2007; MD MD Fox et al., 2005; Shulman et al., 1997). Previous studies have noted cortical BOLD fMRI signal increases at the onset and offset of blocks and events (MD MD Fox et al., 2005; Paret et al., 2014; Uludag, 2008), with a few studies investigating BOLD fMRI signal increases in subcortical networks at the onset of blocks and events (R Li et al., 2021; Kronemer et al., 2022; Setzer et al., 2022). Further research is needed to explore the shared subcortical networks facilitating these sustained and transient attention modulations at block onsets and in response to individual event stimuli, respectively.

In this study, we investigate shared subcortical systems during dynamic modulation of attention across sensory modalities with large sample sizes using both block and event-related fMRI designs. Previous studies have highlighted the early transient signals in subcortical arousal systems, suggesting that a model-free fMRI analysis may be more effective at detecting these signals compared to traditional general linear models, which may not adequately capture such early responses (R Li et al., 2021; Kronemer et al., 2022; Gonzalez-Castillo et al., 2012; Guo et al., 2016). Therefore, we conducted a model-free fMRI analysis for each task included in the study by calculating percentage change in BOLD fMRI signals to identify the subcortical regions activated at task block onsets or in response to individual events, depending on the task design. A conjunction analysis was performed to identify the subcortical regions sharing common early activity across different tasks and sensory modalities. Similarly, we performed a conjunction analysis to identify the shared cortical networks across sensory modalities. Our findings revealed a shared early transient surge in fMRI activity within subcortical arousal systems. Furthermore, we observed similar patterns across sensory modalities in the cortical salience and attention networks. These findings provide new insights into brain mechanisms of arousal and attention and may help identify potential therapeutic targets for restoring arousal and consciousness in patients with neurological disorders.

Methods

Participants and behavioral tasks

We analyzed 3 Tesla (3T) task fMRI data collected from healthy adults while performing 11 different tasks spanning four sensory modalities: vision, audition, taste, and touch. The data were obtained from six publicly available datasets, providing a large overall sample size (Table 1). The datasets included were from the following sources: Washington University-University of Minnesota (WU-Minn) Human Connectome Project (HCP) Young Adult (Barch et al., 2013; Van Essen et al., 2013), University of California Los Angeles (UCLA) Consortium for Neuropsychiatric Phenomics (Poldrack et al., 2016), Glasgow University (Pernet et al., 2015), Jagiellonian University (Czarnecka et al., 2023), and two datasets from Yale University (Dalenberg et al., 2020; Veldhuizen et al., 2020). The HCP dataset provided a significant portion of our data; specifically, task-fMRI data from the HCP 1200 Subjects Data Release were used in this study ($N = 1113$; mean age = 28.8; age range: 22–37 years; females = 606) (WU-Minn 2017). In the visual domain, we examined six tasks, including, the gambling (Delgado et al., 2000), relational processing (Smith et al., 2007), working memory (Caceres et al., 2009; Drobyshevsky et al., 2006), social cognition (Castelli et al., 2000), and motor (Buckner et al., 2011) tasks from the HCP dataset as well as the spatial capacity task (SCAP) (Poldrack et al., 2016) from the UCLA Consortium ($N = 130$; mean age \pm SD = 31.26 ± 8.74 years; age range = 21–50 years; females = 62). For auditory tasks, we analyzed the language task (Binder et al., 2011) from the HCP dataset and the passive listening task (Pernet et al., 2015) from the Glasgow University dataset ($N = 218$; mean age \pm SD = 24.1 ± 7.0 years; age range = NA; females = 101). As for the taste modality, fMRI data from two tasks (Dalenberg et al., 2020; Veldhuizen et al., 2020) collected at Yale University were incorporated in the analysis ($N = 28$; mean age \pm SD = 27.14 ± 4.75 years; age range = 18–37 years; females = 20, and $N = 48$; mean age \pm SD = 27.71 ± 3.94 years; age range = 23–39 years; females = 29). Lastly, in the tactile modality, we analyzed fMRI data of a tactile task (Czarnecka et al., 2023) collected at the Jagiellonian University ($N = 25$; mean age \pm SD = 25.68 ± 3.3 years; age range = 22–32 years; females = 25). Data acquisition procedures at each site were approved by the respective local Institutional Review Boards (IRBs). Informed consent was obtained from all participants in the original studies. The secondary analysis conducted in the present study was approved by the IRB at Yale University. Additional details about the behavioral tasks, fMRI acquisition parameters, and data used in the analysis can be found in the Supplementary Information. The purpose of including different tasks from multiple sensory modalities with large sample sizes was to provide a robust basis for our analyses, allowing identification of shared subcortical systems irrespective of sensory modality, presented stimuli, or task demands.

Depending on the task-design, we analyzed fMRI data either at task block onset to investigate subcortical and cortical networks modulating transitions from baseline blocks to task blocks (block transitions), or at event onset to investigate networks modulating transitions from baseline to events (event transitions). Event transitions were specifically considered for analysis when the time between consecutive events was jittered, while block transitions were examined when a task block was preceded by a baseline block. These criteria led to the analysis of block transitions in nine tasks and to analysis of event transitions in two tasks (Table 1). Information on the number of baseline blocks, task blocks, events, and the number of blocks/events used in the analysis is reported in Table 1. Note that in some cases the number of task blocks analyzed per run was fewer than the number of task blocks per run. This was because we only analyzed task blocks that were preceded by a baseline block (baseline to task transitions), and for some run designs the first task block had no preceding baseline block, while in others, several task blocks were presented sequentially without baseline blocks separating them. More detailed descriptions of the tasks and fMRI data acquisition

Table 1

Overview of the tasks employed in this study, including key design characteristics and analysis-relevant details.

Dataset	Task	Stimulus modality	Analysis type	Duration of task, rest blocks (s)	Blocks of task, rest per run	Number of runs, number of blocks or events analyzed per run	Participants
HCP	Gambling	Visual	Block	28, 15	4, 4	2, 3	1088
HCP	Relational Processing	Visual	Block	16, 16	6, 3	2, 2	1045
HCP	Working Memory	Visual	Block	25, 15	8, 4	2, 3	1091
HCP	Social Cognition	Visual	Block	23, 15	5, 5	2, 4	1054
HCP	Motor	Visual	Block	12, 15	10, 3	2, 2	1086
HCP	Language	Auditory	Event	28, NA	8, NA	2, 12–15 ^a	1054
UCLA	Spatial Capacity	Visual	Event	NA, NA	NA, NA	2, 48	130
Glasgow	Passive Listening	Auditory	Block	8, 12	40, 20	1, 19	217
Yale	Taste Perception I	Taste	Block	36–72, 15	8, 8	4, 7	28
Yale	Taste Perception II	Taste	Block	36–72, 10	12, 12	2, 11	48
Jag. Univ.	Reading Braille	Tactile	Block	4–6, 4–8	72, 7	8, 0–2 ^b	25

^a Each run in the language task contains 4 story blocks and 4 math blocks. Each story block contained one story and each math block contained between 2–3 math problems yielding 12–15 events per run.

^b Of the 8 runs in the tactile Braille reading task, rest-to-tactile task transitions occurred in 2 blocks for 5 runs, in 1 block for two runs, and in 0 blocks for 1 run. *NA: Not Applicable

Data are from the Human Connectome Project (HCP) (Barch et al., 2013; Van Essen et al., 2013), University of California Los Angeles (UCLA) Consortium for Neuropsychiatric Phenomics (Poldrack et al., 2016), Glasgow University (Pernet et al., 2015), Yale University (Dalenberg et al., 2020; Veldhuizen et al., 2020), and Jagiellonian University (Jag. Univ.) (Czarnecka et al., 2023).

parameters are reported in the Supplementary Information.

Preprocessing and artifact rejection

A standard fMRI data preprocessing pipeline was implemented using the Statistical Parametric Mapping (SPM12) toolbox (<http://www.fil.ion.ucl.ac.uk/SPM>) in MATLAB (Mathworks, Inc.). This pipeline was applied to all tasks except those from the HCP dataset. The pipeline comprises three main steps, including motion correction, nonlinear spatial normalization to the standard Montreal Neurological Institute (MNI) space, and spatial smoothing with a Gaussian kernel. For motion correction, functional images acquired in each run were spatially realigned to the first image in that run using 3D rigid-body transformation with three translation and three rotation parameters in the x, y, and z directions. To transform the motion-corrected functional images to MNI space, the structural scan for each participant was coregistered to the mean functional image of the motion-corrected functional images within each run. Next, that structural scan was transformed by non-linear warping to MNI space and the corresponding transformation matrix was applied to the motion-corrected functional images. During this spatial transformation step, functional images from datasets originally acquired with different voxel sizes (UCLA: 4 mm isotropic, Glasgow: 3 mm isotropic, Tactile: 2.1 mm isotropic) were resliced to a consistent voxel size of $2 \times 2 \times 2$ mm³. Functional images from the two Yale datasets were already acquired with a 2 mm isotropic voxel size (as were the HCP data, described below). Finally, the normalized functional images were spatially smoothed with an isotropic Gaussian kernel (FWHM = 6 mm). Because the tactile task had a long repetition time (TR) of 3 s, we applied slice-timing correction in SPM12 before the standard preprocessing steps.

To ensure computational feasibility, we utilized the preprocessed version of the HCP data that had undergone minimal processing using the HCP pipelines (Glasser et al., 2013). The primary preprocessing steps for the HCP data aligned with the standard pipeline we implemented, with one main difference: the HCP pipeline included additional corrections for susceptibility distortions. These corrections required acquisition of field mapping scans, which were not available for the non-HCP datasets, rendering this step infeasible to replicate. Because the preprocessed HCP data (2 mm isotropic voxel size) were unsmoothed, we applied the Gaussian smoothing step (FWHM = 6 mm) from our standard pipeline to maintain consistency with the non-HCP datasets.

Although smoothing affects spatial resolution of fMRI data, it is a

standard preprocessing step prior to statistical analysis that reduces spatial noise and increases the signal-to-noise ratio, thereby improving the reliability of statistical results (Maisog and Chmielowska, 1998; Mikl et al., 2008; Worsley and Friston, 1995). It is generally recommended that the FWHM of the smoothing kernel should be 1.5–3 times the voxel size for effective smoothing (Mikl et al., 2008; Worsley and Friston, 1995; Bijsterbosch et al., 2017; Candemir, 2023; Poldrack et al., 2024). In our study, the voxel size at which the data were acquired varied between 2 and 4 mm isotropic. A FWHM of 6 mm was chosen, as it falls within the recommended range for effective smoothing. Specifically, for the 4 mm isotropic voxel size, the lower bound (1.5 times the voxel size) suggests a 6 mm kernel, while for the 2 mm isotropic voxel size, the upper bound (3 times the voxel size) also results in a 6 mm kernel. This choice ensures that the smoothing kernel is appropriately matched to the varying voxel sizes across the datasets, balancing noise reduction while minimizing the impact on spatial specificity for small regions of interest.

For both HCP and non-HCP tasks, runs were excluded from the analysis if transient head movement exceeded 2 mm of translation and 1° of rotation in any of the three directions. These criteria resulted in excluding 2506 runs out of 13,643 runs (18.37 %) from the analysis. Information on excluded runs per task are reported in the Supplementary Information (Supplementary Table S1). To further remove spatial and temporal noise from the data, the smoothed BOLD functional images were next passed through a five step denoising procedure as in previous work from our group (R Li et al., 2021; Kronemer et al., 2022; Guo et al., 2016). Data were (1) grey matter masked to exclude non-grey matter voxels using a standard gray matter mask from MarsBaR (<http://marsb.sourceforge.net/>) modified to include the midbrain and pons (The mask volume in MNI space is publicly available here: https://github.com/BlumenfeldLab/Khalaf-et-al_2025), (2) filtered using a 1/128 Hz high-pass filter, (3) corrected for motion artifacts by utilizing a general linear model with the six rigid-body motion parameters estimated during functional image realignment to regress out motion, (4) subjected to rejection of individual volumes if the volume-to-volume root mean squared difference in BOLD signal (DVARs) at a certain time point exceeded a threshold of 5 (Power et al., 2012; Smyser et al., 2010), and (5) subjected to rejection of individual volumes if instantaneous changes in head position, known as framewise displacement (FD) exceeded a threshold of 0.3 at a certain time point (Power et al., 2012; Smyser et al., 2010). FD is calculated as the sum of the absolute values of change in head movement among the six rigid-body motion parameters.

Percent change analysis

To identify the subcortical and cortical networks showing transient BOLD changes at block and event onset, we performed a model-free fMRI analysis by calculating the percent change in BOLD signal across time for the whole brain as in previous work (R Li et al., 2021; Kronemer et al., 2022; Bai et al., 2010; Guo et al., 2016). Through the percent change analysis, we obtained percent change brain maps and percent change time courses showing the transient BOLD changes associated with block and event transitions. The tasks included in the analysis utilized four different TR values as follows: 0.72 s (6 HCP tasks), 1 s (2 Yale tasks), 2 s (2 Glasgow and UCLA tasks), and 3 s for the tactile task. Percentage change analyses were conducted using the original TRs at which the tasks were acquired, and timing was later adjusted as described below. All analyses were completed in MATLAB using custom functions as well as functions from SPM12.

It should be noted that the magnitude of the percentage change in fMRI signals depends on the method used for calculation. The approach used here and in several previous studies is to calculate the percent change relative to the mean of the entire run, which tends to result in smaller percent change values (R Li et al., 2021; Kronemer et al., 2022; Guo et al., 2016; XX Bai et al., 2010; McCafferty et al., 2023). In contrast, if percent change is calculated relative to the baseline periods, the values may be larger (Chee et al., 2003; Grill-Spector et al., 2004; Kanwisher et al., 1997; Kanwisher et al., 1998; Tambini et al., 2010). Finally, percent change can be calculated by dividing general linear model beta values associated with the stimulus by the model constant, providing a single value rather than a time course, and resulting in different values compared to the time-course approach (Angsturm et al., 2024; Gläscher, 2009; Williams et al., 2014; Williams et al., 2016). Another consequence of using the percent change relative to the mean of the entire run is that if task periods occupy more time than rest periods in a block design, then the mean across the entire run will lie closer to the task period mean, causing values in the rest periods to appear negative.

Percent change brain maps

The BOLD percent change was calculated for the time course of each

voxel relative to the mean BOLD signal of that voxel across the entire run. The BOLD volume corresponding to the onset of a specific block/event was defined as the volume that immediately preceded the block/event onset. A block/event epoch included all volumes corresponding to the 15 s before the block/event onset to the 15 s after. Epochs were averaged across blocks/events within the same run then across runs, resulting in a single 30-second-long average percent change epoch for each subject. Temporal resolution of the percent change brain map calculations was retained at the original acquisition TR with the exception of tactile task which was upsampled from TR=3 s to TR=2 s. Specifically, the upsampling was performed on the subject-level percentage change epochs using linear interpolation. Spatiotemporal cluster-based permutation testing was applied to these epochs across subjects for each task to identify the statistically significant voxels and time points compared to the baseline before the block/event onset (see Statistical Analysis section below).

Anatomical localization and percent change time courses

To precisely localize the observed subcortical activity on the structural MRI template, we used regions of interest (ROIs) from several published *a priori* anatomical atlases. We used the Harvard ascending arousal network (AAN) atlas (Edlow et al., 2024) for brainstem nuclei, the Morel atlas (Niemann et al., 2000) for thalamic nuclei, the basal ganglia human area template (BGHAT) atlas (Prodoehl et al., 2008) for basal ganglia, as well as an atlas of basal forebrain and hypothalamus nuclei (Neudorfer et al., 2020). For the amygdala, we used the amygdala ROI available through the MNI PD25 atlas (Xiao et al., 2017). These atlases were used for anatomical localization in the figures, and in Table 2.

In addition to anatomical localization, we used the anatomical atlases to define ROIs for time course analysis in two regions showing shared changes across all modalities, represented by the midbrain reticular formation (AAN atlas) and the thalamic intralaminar central lateral nucleus (Morel atlas). To obtain the time-course of each ROI per subject, we averaged the percentage change time courses across voxels within that ROI using the data from the subject-level percent change maps (see *Percent Change Brain Maps* section). For percent change time

Table 2

Early transient BOLD fMRI changes in different subcortical ROIs across sensory modalities within four seconds from block/event onset.

Region	ROI	Increases or Decreases in Each Modality				Changes Across Modalities	
		Visual (L, R)	Auditory (L, R)	Taste (L, R)	Tactile (L, R)	Shared Incr. (L, R)	Shared Decr. (L, R)
Pons	Locus coeruleus	0,0	+,+	+,+	0,0	2,2	0,0
	Parabrachial nucleus	0,+	+,+	+,+	0,0	2,3	0,0
	Pontine nucleus oralis	0,+	+,+	+,+	0,0	2,3	0,0
Midbrain	Dorsal raphe	+	+	0	0	2	0
	Midbrain reticular formation	+,+	+,+	+,+	+,+	4,4	0,0
	Pedunculopontine tegmental nucleus	0,+	+,+	0,0	+,+	2,3	0,0
	Superior colliculi	+,+	+,+	+,+	+,0	4,3	0,0
	Ventral tegmental area	+	+	0	0	2	0
Hypothalamus	Lateral hypothalamus	+,+	+,0	+,0	0,0	3,1	0,0
	Posterior hypothalamus	+,+	+,0	+,+	0,0	3,2	0,0
Basal forebrain/ Amygdala	Amygdala	0,0	-,0	+,+	-,	1,1	2,1
	Nucleus Basalis	0,0	-,0	+,+	0,0	1,1	1,0
	Central lateral nucleus	+,+	+,+	+,+	+,+	4,4	0,0
Thalamus	Centromedian nucleus	+,+	+,+	+,+	0,+	3,4	0,0
	Mediodorsal nucleus	+,+	+,+	+,+	+,+	4,4	0,0
	Ventral lateral nucleus	+,+	+,+	+,+	+,+	4,4	0,0
	Ventral medial nucleus	+,+	+,+	+,+	0,+	3,4	0,0
	Caudate	0,+	0,0	0,0	+,+	1,2	0,0
Basal Ganglia	Putamen	0,0	-,	+,+	-,	1,1	2,2
	Globus pallidus	+,+	-,	+,+	-,	2,2	2,2
	Nucleus accumbens	0,0	0,0	0,0	0,+	0,1	0,0
	Subthalamic nucleus	+,+	+,+	+,+	0,0	3,3	0,0

In the first four columns, for each modality +, -, 0 denote statistically significant increases, decreases, or no change, respectively at four seconds after block/event onset in a given ROI. Changes are shown for left (L) and right (R) sides for bilateral ROIs. The dorsal raphe and ventral tegmental area were single midline ROIs without left or right sides, so only single values are shown for those two ROIs. The right two columns show total number of modalities with significant increases (Incr.) or decreases (Decr.) for each ROI.

course calculations for these two ROIs, subject-level percentage change epochs for all tasks were upsampled through applying linear interpolation to a common TR of 0.72 s (HCP sampling rate). To identify the statistically significant time points compared to the baseline before the block/event onset, temporal cluster-based permutation testing was applied to the ROI time courses across subjects as described in the temporal analysis portion of the next section.

Statistical analysis

Our overall approach was to first perform separate statistical analyses for each of the 11 tasks in each modality, and to then perform conjunction and disjunction analyses across sensory modalities. Spatiotemporal cluster-based permutation testing was employed to identify voxels and time points showing statistically significant changes in post block/event percent change signals compared to the baseline prior to block/event onset (Kronemer et al., 2022). This approach overcomes the multiple comparisons problem through calculating a single test statistic for the entire spatiotemporal percent change data grid instead of evaluating the statistical significance at each voxel-time point pair (Maris and Oostenveld, 2007). No assumptions are made about the hemodynamic response time course, thus avoiding problems where time course models may not fit the data in some brain regions (Gonzalez-Castillo et al., 2012; Guo et al., 2016; Handwerker et al., 2004). Additionally, this nonparametric approach does not have assumptions about the distribution of the data which limits false positive rates, especially in high-dimensional data such as fMRI, unlike parametric methods that may incorrectly model functional MRI data, leading to higher false positive rates than their nominal rates (Bansal and Peterson, 2018). The cluster-based permutation statistical approach implemented in this study was adapted from the Mass Univariate ERP Toolbox (Groppe et al., 2011) in MATLAB.

Spatiotemporal analyses

Spatiotemporal statistical analysis was conducted using the original TRs at which the tasks were acquired, except for the tactile task, for which the percentage change data were upsampled to a TR of 2 s prior to statistical analysis, as already described. Given the high dimensionality of fMRI data, to improve computational efficiency we implemented two versions of our statistical analysis (Kronemer et al., 2022); a high-resolution version to identify statistically significant changes in subcortical areas, as well as a lower-resolution version to identify statistically significant changes in the whole brain. In the high-resolution subcortical statistical analysis, the voxel size was preserved at 2 mm isotropic, but to speed processing the voxels included in the analysis were restricted to the subcortical grey matter voxels in the brainstem, thalamus, basal ganglia, basal forebrain and hypothalamus. In the lower-resolution whole-brain analysis, all the voxels in the grey matter were included, adding the cerebral cortex and cerebellum, but increasing the voxel size from $2 \times 2 \times 2$ to $6 \times 6 \times 6$ mm³ to improve computational efficiency. Both the high-resolution subcortical and low-resolution whole-brain statistical analyses were applied to the percent change epochs across subjects in a given task to identify the statistically significant voxels and time points post block/event onset compared to the baseline before the block/event onset. The baseline was defined as the 6 s prior to block/event onset.

For the whole brain analysis, spatial resolution was reduced by combining spatially adjacent $2 \times 2 \times 2$ mm³ grey matter voxels to form larger $6 \times 6 \times 6$ mm³ voxels. Specifically, the central voxels for each of the $6 \times 6 \times 6$ mm³ lower-resolution voxels were defined as the original $2 \times 2 \times 2$ mm³ voxels positioned with exactly 2 intervening voxels until the next central voxel in the x, y, and z directions. Next, all adjacent voxels sharing a face, edge, or vertex with a central voxel were found. These adjacent voxels combined with the central voxel formed the $6 \times 6 \times 6$ mm³ voxel. Finally, the BOLD percent change signal value within

each of the lower spatial resolution $6 \times 6 \times 6$ mm³ voxels was determined by computing the mean BOLD signal across all $2 \times 2 \times 2$ mm³ voxels within each of the lower resolution $6 \times 6 \times 6$ mm³ voxels. If all the adjacent voxels for a certain central voxel were located in the grey matter, the $6 \times 6 \times 6$ mm³ voxel would include 27 (33) of the $2 \times 2 \times 2$ mm³ voxels. Otherwise, the larger voxel would combine all available adjacent voxels resulting in a non-cuboidal shaped voxel.

Cluster-based spatiotemporal permutation analysis was performed as in prior work (Kronemer et al., 2022) by generating the spatiotemporal cluster null distribution through 5000 permutation iterations. For each permutation, the mean of the 6-second percent change baseline at a specific voxel and the percent change value of that voxel at the tested time point were randomly shuffled based on the direction of subtraction (time point minus baseline or baseline minus time point) for each participant. Next, a paired, two-tailed *t*-test compared the permuted values across participants to identify the statistically significant voxels at each tested time point ($p < 0.05$) from −15 s before block/event onset up to 15 s afterwards.) Statistically significant spatiotemporal clusters were formed by considering spatial and temporal adjacencies. Negative and positive clusters were created independently. Spatially adjacent voxels were defined as statistically significant voxels (in the same direction) sharing a face, edge, or vertex. Temporal adjacency was found if a voxel was statistically significant (in the same direction) at two or more sequential time points. For each spatiotemporal cluster, the summed absolute value of *t*-values was computed across all voxels and time points belonging to that cluster. The largest negative and positive cluster determined separately by summed absolute value of *t*-values was selected from each permutation. Because the positive and negative values were randomly shuffled, we assumed symmetry in the permutation distribution, so we only retained negative clusters and created a one-sided distribution to reduce computations. Therefore, the *p*-value threshold was set at 0.025 (equivalent to 0.05 in a two-sided distribution). For each permutation, we retained only the negative cluster with the largest absolute *t*-value and collected these values across 5000 permutations to create a permutation distribution. After generating the spatiotemporal cluster null distribution, the spatiotemporal cluster forming analysis described above was applied to the unpermuted data. Positive and negative clusters were identified separately, and summed *t*-values with absolute value above the top 2.5 % of the permutation distribution were considered significant.

The cluster-based spatiotemporal analysis was performed separately on the whole brain at $6 \times 6 \times 6$ mm³ resolution, and on subcortical regions at $2 \times 2 \times 2$ mm³ resolution. Importantly, the high resolution $2 \times 2 \times 2$ mm³ analysis improved the spatial identification of small subcortical regions, but did not add any new regions to the final conjunction analysis results that were not seen in the whole brain lower resolution analysis. Therefore, for display purposes when showing results of whole brain $6 \times 6 \times 6$ mm³ resolution analysis on cortical brain slices, we superimposed the $2 \times 2 \times 2$ mm³ resolution results for subcortical structures on the same slices/surfaces (e.g. Figs. 3, 5 and Supplementary Presentations S1, S3, and S4).

Temporal analyses

We implemented a temporal cluster-based permutation test, which is an adapted version of the spatiotemporal cluster-based permutation test described above to identify the statistically significant changes in the ROI percent change time courses (Kronemer et al., 2022). In particular, the cluster-forming approach in the temporal analysis considered only temporal adjacency unlike the spatiotemporal version, which considers both spatial and temporal adjacencies to form spatiotemporal clusters. For each ROI, the temporal cluster-based permutation test was applied to the percent change time courses across subjects for a given task to identify the statistically significant time points post block/event onset compared to the baseline before the block/event. The baseline was defined as the 6 s prior to block/event onset. As was already mentioned,

before applying temporal statistical analysis, ROI percentage change data for all tasks were resampled to a common TR of 0.72 s (Fig. 1C, D; Supplementary Presentation S2).

Subcortical and whole-brain conjunction and disjunction analyses

Binary conjunction analysis

To identify the shared subcortical and cortical networks across tasks and sensory modalities, we performed a binary conjunction analysis at each of the time points within an epoch (15 seconds pre and post block/event onset) across tasks. We refer to this as binary conjunction because a voxel was either included or not in the results based on all-or-none statistical criteria. For a voxel to be included in this conjunction, it had to show statistically significant changes (based on permutation testing) in the same direction (i.e., positive or negative) across all modalities and across all 11 tasks at the same time point. Voxels with both positive and negative changes at a given time point were not included in the binary conjunction brain maps. The binary conjunction analysis was performed separately for the high-resolution subcortical and lower-resolution whole-brain statistical results from the permutation testing (Fig. 1A, B; Figure 3A; Supplementary Presentation S1).

To standardize the analysis TR for conjunction it was necessary to ensure the volumes were temporally aligned at each time point. As mentioned earlier, the tasks included in the analysis utilized four different TR values, including, 0.72 s (6 HCP tasks), 1 s (2 Yale tasks), 2 s (2 Glasgow and UCLA tasks), and 3 s for the tactile task, with only the latter (tactile) TR upsampled from 3 to 2 s by linear interpolation. To minimize the need for additional upsampling and creation of new data points that were not physically acquired in the scanner, we selected a common TR of 2 s for conjunction analysis across tasks. Specifically, permutation based spatiotemporal cluster-based statistical analysis was done at the original TR for each task, except for the tactile task, as already described, then for conjunction analysis, we used the volume closest in time to the 2 s TR time points for any tasks with higher (0.72 or 1 s) sampling rates.

Graded conjunction analysis

The binary conjunction approach had strict inclusion criteria, meaning a region would only be included in the conjunction if it was significant across all sensory modalities and tasks at the same time points. To identify regions that are statistically significant across most sensory modalities but not all of them, we introduced a graded conjunction method, to identify significant voxels in 1, 2, 3 or all 4 modalities. Graded conjunction analysis was implemented in the following two ways: 1. On a voxel-by-voxel basis, similar to binary conjunction; 2. In a *prior* defined anatomical ROIs.

For voxel-wise graded conjunction analysis, we began with binary conjunctions within each sensory modality to identify voxels sharing increases or decreases at the same time point, using the same binary approach already described (with the exception of the tactile modality which had only one task, so no within-modality conjunction was needed). This process yielded binary maps for statistically significant increases or decreases across tasks for each sensory modality (Supplementary Presentation S3). Subsequently, these maps were aggregated separately for increases and decreases, with voxel values indicating the number (1 to 4) of sensory modalities sharing statistically significant changes in the same direction (i.e., positive or negative) at each time point (Figure 2; Fig. 3B, C; Supplementary Presentation S1).

For ROI-based graded conjunction analysis, we used the defined anatomical ROIs based on atlases listed above (see *Anatomical Localization* section). We evaluated each subcortical ROI to determine whether it overlapped with increases or decreases in the binary conjunction maps for each modality (Table 2, left four columns). This was done using a

criterion where if >50 % of the ROI overlapped with significant changes in a given modality, this was counted as an increase or decrease for that ROI. To report the graded conjunction of changes across modalities, we then listed the number of modalities sharing increases or decreases for each ROI (Table 2, right two columns).

Disjunction analyses

We performed exclusive disjunction analyses to identify subcortical and cortical regions unique for each sensory modality. Similar to the conjunction analyses, we performed the disjunction analyses separately on the high-resolution subcortical and lower-resolution whole-brain statistical maps (Figure 4; Figure 5; Supplementary Presentation S4). We first obtained binary conjunction maps across tasks within each sensory modality to identify voxels sharing increases or decreases at the same time point, as already described. We then performed disjunction analysis comparing each modality to the other three. For a voxel to be included in the disjunction of a specific sensory modality, it had to show statistically significant changes in a specific direction (i.e., positive or negative) only in the binary conjunction maps of that sensory modality but not in the binary conjunction maps of any of the other three modalities at the same time point.

Brain map visualization

The conjunction and disjunction maps we obtained were overlaid on a 100 μ m 7T MRI structural scan of an ex vivo human brain (Edlow et al., 2019) for improved visualization and localization of the subcortical structures of interest. Supplementary Figures S1 and S2 confirm the alignment between the average anatomical scan of the 1561 subjects included in the study and the 100 μ m 7T MRI structural template. These maps were also plotted on the fsaverage FreeSurfer (<https://surfer.nmr.mgh.harvard.edu/>) inflated brain surface (left hemisphere: lh.inflated surface; right hemisphere: rh.inflated surface) to show the spatial extent of the shared cortical networks as well as the cortical networks unique to each sensory modality.

Time-Course conjunction analysis

We performed a binary conjunction analysis on the ROI time courses to identify the time points sharing common significant changes across all modalities and tasks relative to the baseline before block/event onset for each subcortical ROI (see *Temporal Analyses* section above). Similar to the conjunction analysis applied to brain maps, for a time point to be included in the conjunction, it had to show statistically significant changes in the same direction (i.e., positive, or negative) across all modalities and all 11 tasks at the same time point. The binary conjunction was performed at each time point spanning from -15 to 15 s relative to the block/event onset. For display purposes (Fig. 1C, D), the mean percent change time course for each ROI was calculated by first averaging across subjects within each task, and these time courses were then averaged across all 11 tasks.

Results

Previous studies have mainly focused on the role of cortical networks in top-down and bottom-up dynamic modulation of attention (Corbetta and Shulman, 2002; Dosenbach et al., 2008; Fortenbaugh et al., 2017; Helfrich et al., 2019). Meanwhile, subcortical arousal structures are mainly known for their role in controlling long-lasting states such as sleep-wake cycles (Steriade and McCarley, 2010), but their role in dynamic modulation of attention has been increasingly studied recently (Sarter and Lustig, 2020; R Li et al., 2021; Kronemer et al., 2022). In the current study, we aim to investigate a shared transient pulse of activity in subcortical arousal systems that we found occurs with modulation of attention across 11 different tasks spanning four sensory modalities,

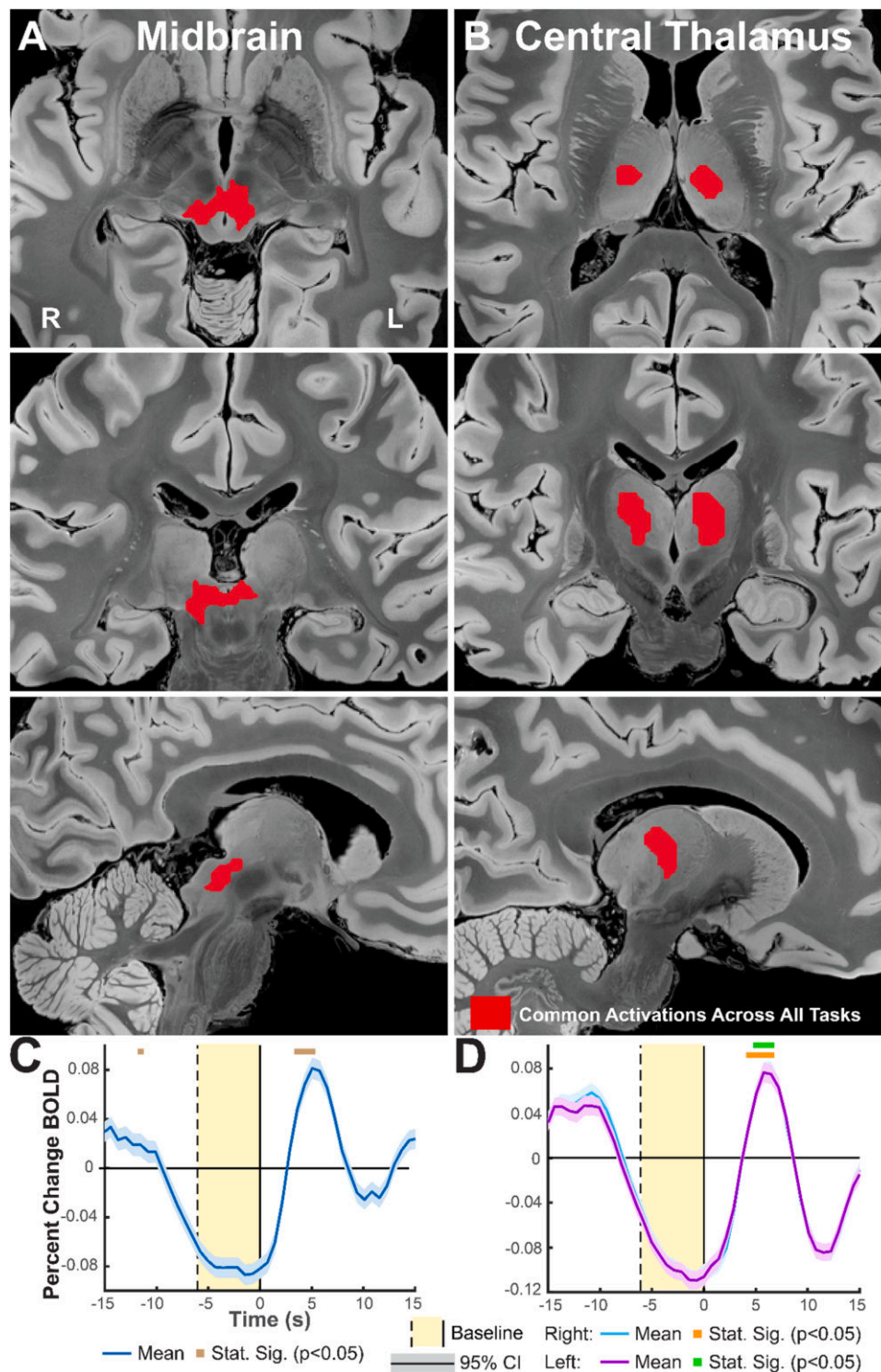


Fig. 1. Midbrain and central thalamus show shared subcortical early activations (increases), observed in 11 tasks across four sensory modalities, including, vision, audition, taste, and touch. These shared activations reached statistical significance within four seconds from block/event onset. Cluster-based permutation testing ($p < 0.05$) was employed to identify the statistically significant changes in percentage change BOLD brain maps and time courses with respect to the baseline before block/event onset for each sensory task. Binary conjunction analysis was then applied across all tasks to identify subcortical regions and time points sharing activations/deactivations across tasks and sensory modalities. (A) Axial, coronal, and sagittal MRI slices in the midbrain showing the spatial extent of the observed shared activations 4 s after stimulus onset, mainly centered on the midbrain reticular formation (MRF). No shared deactivations were seen. (B) Axial, coronal, and sagittal MRI slices showing the spatial extent of the observed activations in the thalamus 4 s after stimulus onset, centered on the intralaminar central lateral (CL) nucleus. (A, B) for additional brain slices and time points see Supplementary Presentation S1. (C, D) Mean ($\pm 95\%$ confidence interval, CI) percent change BOLD time courses across the 11 tasks from two anatomical ROIs, MRF (C) and CL (D), obtained from the Harvard Ascending Arousal Network atlas and the Morel atlas, respectively. Note that the Percent Change BOLD signal appears negative during the Baseline (non-task) periods because percent change was calculated with respect to the mean BOLD signal for the entire run, including both task and non-task blocks (see Methods). The significant (Stat. Sig.) time points shared across tasks

(permutation based statistics followed by conjunction analysis), marked on the top of the time courses, began 4 s after block/event onset in both the MRF and thalamic CL. Data are from 11 tasks obtained across a total of 1561 participants.

including, vision, audition, taste, and touch. We used large sample sizes to ensure robustness of the results and to confirm that the observed networks are independent of the task design, type, or demands. This approach allows better isolation of brain activity due to dynamic transitions in attention from the activity due to particular stimuli/tasks. We performed a model-free fMRI analysis by calculating percent change in BOLD fMRI signals with respect to the mean of each fMRI run. To identify the statistically significant changes in percent change BOLD brain maps and time courses with respect to the baseline just prior to transitions in attention, we employed cluster-based permutation testing ($p < 0.05$). Binary and graded conjunctions were performed on the statistical brain maps and time courses to identify the shared subcortical and cortical regions across sensory modalities. Disjunction analyses were applied to the statistical brain maps to identify unique cortical and subcortical regions for each sensory modality.

Binary conjunction analysis showed a shared transient pulse of subcortical fMRI increases across all sensory modalities and tasks in the midbrain and central thalamus within four seconds from the stimulus onset (Fig. 1.A, 1.B). These increases were centered mainly on the midbrain reticular formation (MRF) and thalamic intralaminar central lateral nucleus (CL) which are key subcortical structures for arousal and attention modulation (Steriade and McCarley, 2010; R Li et al., 2021; Schiff et al., 2013; S S Kinomura et al., 1996; Edlow et al., 2024). Shared fMRI increases across modalities extended into adjacent anatomical regions of the midbrain tegmentum and into other nearby thalamic nuclei

such as the mediodorsal nucleus and ventrolateral nucleus bordering thalamic CL (See Supplementary Presentation S1 for binary conjunction maps in additional brain slices and time points). To investigate the timing of these changes, we performed a conjunction analysis of the mean time course of percent change fMRI signals in the MRF and thalamic CL nucleus across all tasks (Fig 1.C, D). This demonstrated a shared significant transient increase in both regions across all sensory modalities and tasks within four seconds from the stimulus onset, which remained significant for an additional 2–4 s before returning towards baseline. Thus, a transient pulse of fMRI activation was seen most consistently in the midbrain reticular formation and central thalamus during transitions of attention in a large data set across perceptual modalities and tasks. A detailed breakdown of the MRF and CL time courses for each task, sensory modality, and analysis type (block/-event-related) is provided in Supplementary Presentation S2. These time courses show that, although there are small variations in the magnitude of the percent change BOLD signal across tasks, all tasks exhibit statistically significant and similar transient increases at overlapping time points.

Our binary conjunction approach employed stringent inclusion criteria where a region could be included in the conjunction only if it showed significance across all sensory modalities at the same time point. To pinpoint regions statistically significant across some sensory modalities, but not necessarily all of them, we conducted graded conjunction analyses. The graded conjunction analysis revealed subcortical

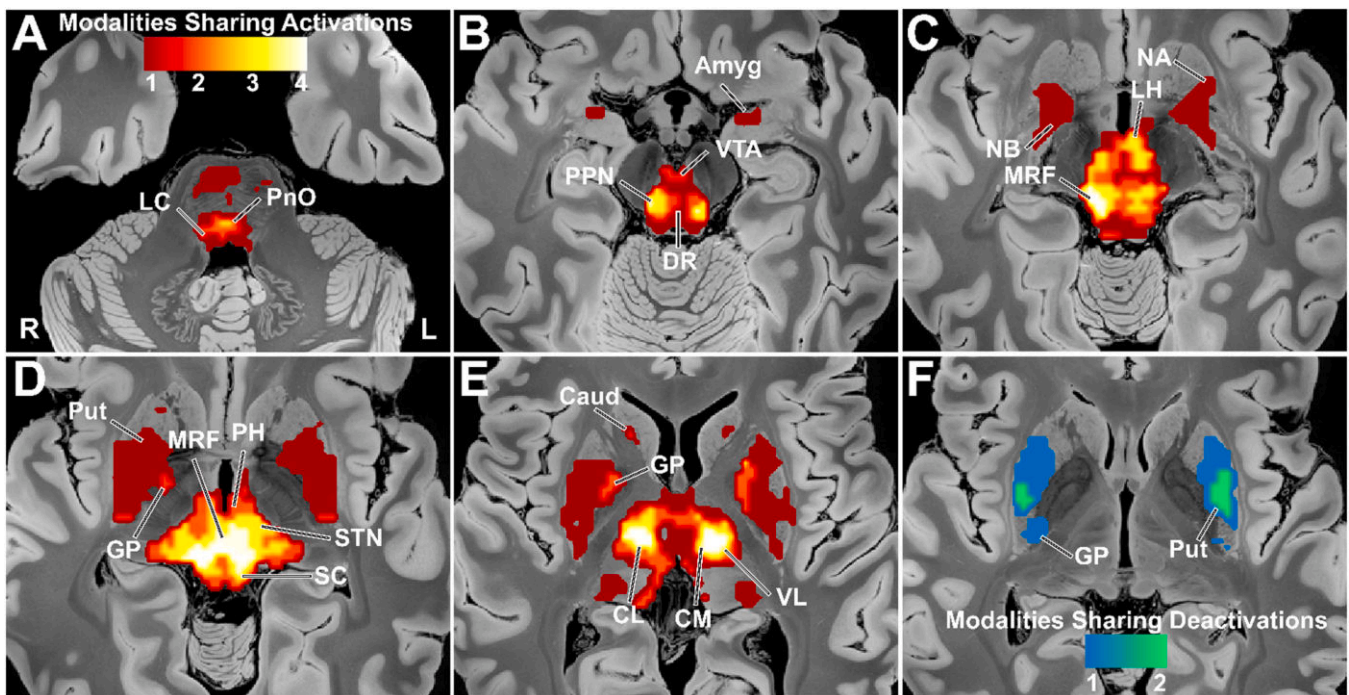


Fig. 2. Graded conjunction analysis revealed additional subcortical changes shared less consistently across sensory modalities. This method, which is less stringent than binary conjunction, highlights shared activations (increases) and deactivations (decreases) even if they do not occur across all sensory modalities. The activations and deactivations shown are from four seconds after block/event onset. Spatiotemporal cluster-based permutation testing ($p < 0.05$) was employed to identify the statistically significant changes in percentage change BOLD brain maps with respect to the baseline before block/event onset for each task, and binary conjunction revealed shared changes within each of the four sensory modalities. Graded conjunction analysis was then applied across the four sensory modalities to identify subcortical regions with shared activations/deactivations, and shared changes were graded from 0 to 4 based on number of modalities shared. (A – E) shared subcortical activations; (F) shared subcortical deactivations. For additional brain slices and time points of the graded conjunction analysis please see Supplementary Presentation S1. Locus ceruleus (LC), pontine nucleus oralis (PnO), pedunculopontine tegmental nucleus (PPN), ventral tegmental area (VTA), dorsal raphe (DR), amygdala (Amyg), midbrain reticular formation (MRF), lateral hypothalamus (LH), nucleus basalis (NB), nucleus accumbens (NA), posterior hypothalamus (pH), subthalamic nucleus (STN), superior colliculus (SC), caudate nucleus (Caud), thalamic central lateral nucleus (CL), thalamic centromedian nucleus (CM), thalamic ventrolateral nucleus (VL). Same data and participants as in Fig. 1.

increases and decreases less consistently shared across modalities, not detectable through the strict binary conjunction that required the activity to be shared across all tasks. Through the graded conjunction analysis, we found early fMRI changes after stimulus onset overlapping

several subcortical structures, including those in the pons, midbrain, hypothalamus, basal forebrain, amygdala, thalamus and basal ganglia (Fig. 2 and Table 2; see also Supplementary Presentation S1 for graded conjunction maps in additional brain slices and time points). In the pons,

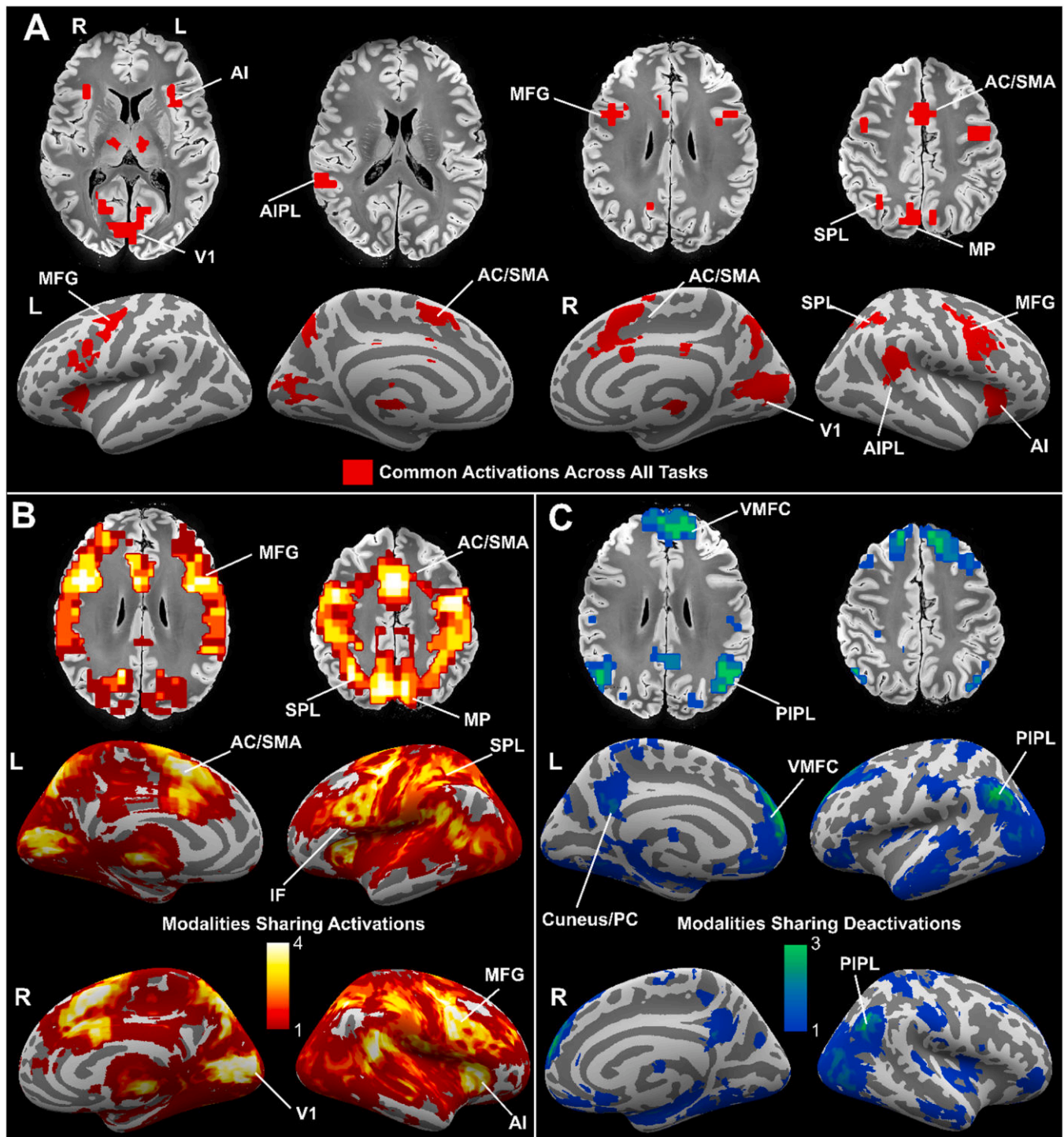


Fig. 3. Shared cortical fMRI activations (increases) and deactivations (decreases) four seconds after block/event onset, obtained from whole brain analysis. (A) Binary conjunction analysis required shared activations/deactivations across the 11 tasks and four sensory modalities. Top row, axial slices; bottom row, surface views. (B) Graded conjunction analysis showing number of modalities sharing cortical activations (significant fMRI increases) across the four sensory modalities. Top row, axial views; bottom rows surface views. (C) Graded conjunction analysis for deactivations across modalities. Top row, axial views; bottom rows surface views. For additional brain slices and time points of the binary and graded conjunction analyses please see Supplementary Presentation S1. Anterior insula (AI), anterior cingulate/supplementary motor area (AC/SMA), primary visual cortex (V1), anterior inferior parietal lobule (AIPL), superior parietal lobule (SPL), medial parietal cortex (MP), middle frontal gyrus (MFG), inferior frontal gyrus/frontal operculum (IF), ventral medial frontal cortex (VMFC), posterior cingulate (PC), and posterior inferior parietal lobule (PIPL). Same data and participants as in Fig. 1.

shared increases were noted in at least two sensory modalities 4 s after stimulus onset in the locus coeruleus, parabrachial nucleus, and pontine nucleus oralis. In the midbrain, in addition to the MRF, early shared increases were observed in the dorsal raphe, pedunculopontine tegmental nucleus, superior colliculi, and ventral tegmental area. In the thalamus, in addition to CL, consistent increases were seen in all modalities in adjacent central thalamic regions of the mediodorsal and ventrolateral nuclei. The nearby centromedian and ventral medial nuclei also showed increases in three or four modalities. Increases in at least two modalities were also seen in the lateral and posterior hypothalamus, as well as in the basal ganglia caudate, globus pallidus and subthalamic nucleus. Increases in only one modality were seen in the amygdala, nucleus basalis, nucleus accumbens and putamen. fMRI decreases were less consistently seen in subcortical structures at early times, with shared decreases seen across two sensory modalities in the amygdala, putamen and globus pallidus; and in one modality in the nucleus basalis.

To comprehensively delineate the brain networks outside subcortical regions that participate during transitions in attention across sensory modalities, we performed a whole-brain binary conjunction analysis to identify the involved cortical networks. The whole-brain conjunction

showed transient cortical increases at early times in detection, arousal and salience networks, including bilateral visual cortex, bilateral anterior insula and bilateral anterior cingulate/supplementary motor area (Fig. 3A). Early increases were also observed in attention and executive control networks, including the right anterior inferior parietal lobule, right superior parietal lobule, bilateral medial parietal cortex, and bilateral middle frontal gyrus (Fig. 3A). For cortical regions, we also conducted a graded conjunction analysis to identify fMRI changes present in some but not all sensory modalities. The graded conjunction analysis enabled identification of additional bilateral cortical regions showing less consistent increases across modalities at early times including the opercular part of the inferior frontal gyrus (Fig. 3B). In addition, although no early shared cortical fMRI decreases were observed across all sensory modalities, the graded conjunction analysis revealed early decreases in at least three modalities in default mode network areas, including the ventral medial prefrontal cortex, posterior cingulate/precuneus, and posterior inferior parietal lobule (Fig. 3C; see also Supplementary Presentation S1 for binary and graded conjunction maps of shared cortical changes in additional brain slices and time points).

To further validate our approach investigating shared changes across

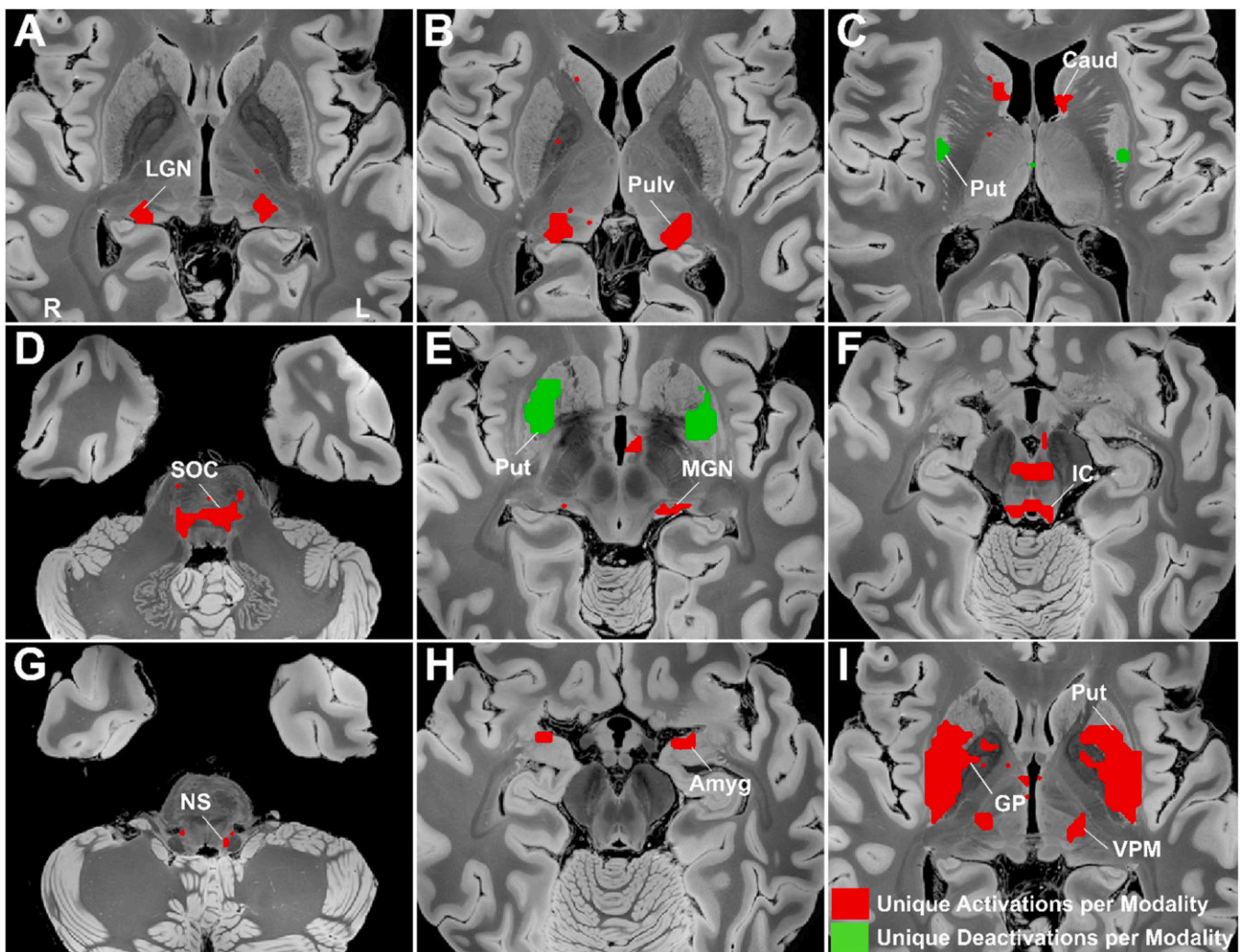


Fig. 4. Unique subcortical activations (increases) and deactivations (decreases) for each of the four sensory modalities (vision, audition, taste, and touch) observed four seconds after block/event onset. Exclusive disjunction analysis identified statistically significant subcortical changes present in each modality alone but in none of the other sensory modalities. (A, B) Visual disjunction analysis. (C) Tactile disjunction analysis. (D – F) Auditory disjunction analysis. (G – I) Taste disjunction analysis. For additional brain slices and time points of the disjunction analyses for each modality please see Supplementary Presentation S4. Lateral geniculate nucleus (LGN), pulvinar (Pulv), putamen (Put), caudate nucleus (Caud), superior olivary nuclear complex (SOC), medial geniculate nucleus (MGN), inferior colliculus (IC), nucleus solitarius (NS), amygdala (Amyg), globus pallidus (GP), ventral posterior medial nucleus (VPM). Same data and participants as in Fig. 1.

sensory modalities, we also analyzed changes specific to each modality. As already described for the binary and graded conjunction analyses, we began by constructing binary conjunction maps across tasks within each modality to obtain changes for the four modalities (see Supplementary Presentation S3). We then used exclusive disjunction analyses to identify changes unique for each sensory modality. This approach retained only voxels that showed statistically significant increases or decreases for one modality but no others at each location in the brain. We found expected sensory modality-specific changes at early times after stimulus onset in both subcortical and cortical regions. Thus, the subcortical disjunction analysis revealed fMRI increases in the lateral geniculate nucleus and pulvinar exclusively for visual tasks (Fig. 4A, B); increases in the superior olivary complex, medial geniculate nucleus, and inferior colliculus as well as decreases in the putamen exclusively for auditory tasks (Fig. 4D - F); increases in the nucleus solitarius, ventral posterior medial

nucleus, amygdala and regions of the basal ganglia exclusively for the taste tasks (Fig. 4G - I); and increases in the caudate nucleus as well as decreases in a portion of the putamen for tactile tasks (Fig. 4C). Cortical disjunction analyses likewise showed mainly expected changes unique to each sensory modality at early times after stimulus onset. These included increases in the fusiform gyrus and intraparietal sulcus for visual tasks (Fig. 5A, B); increases in primary auditory cortex for auditory tasks (Fig. 5C, D); increases in the anterior insula and other regions for taste tasks (Fig. 5E, F); and increases in primary somatosensory cortex along with changes in several other cortical regions for the tactile tasks (Fig. 5G, H; see also Supplementary Presentation S4 for disjunction maps for each sensory modality in additional brain slices and time points).

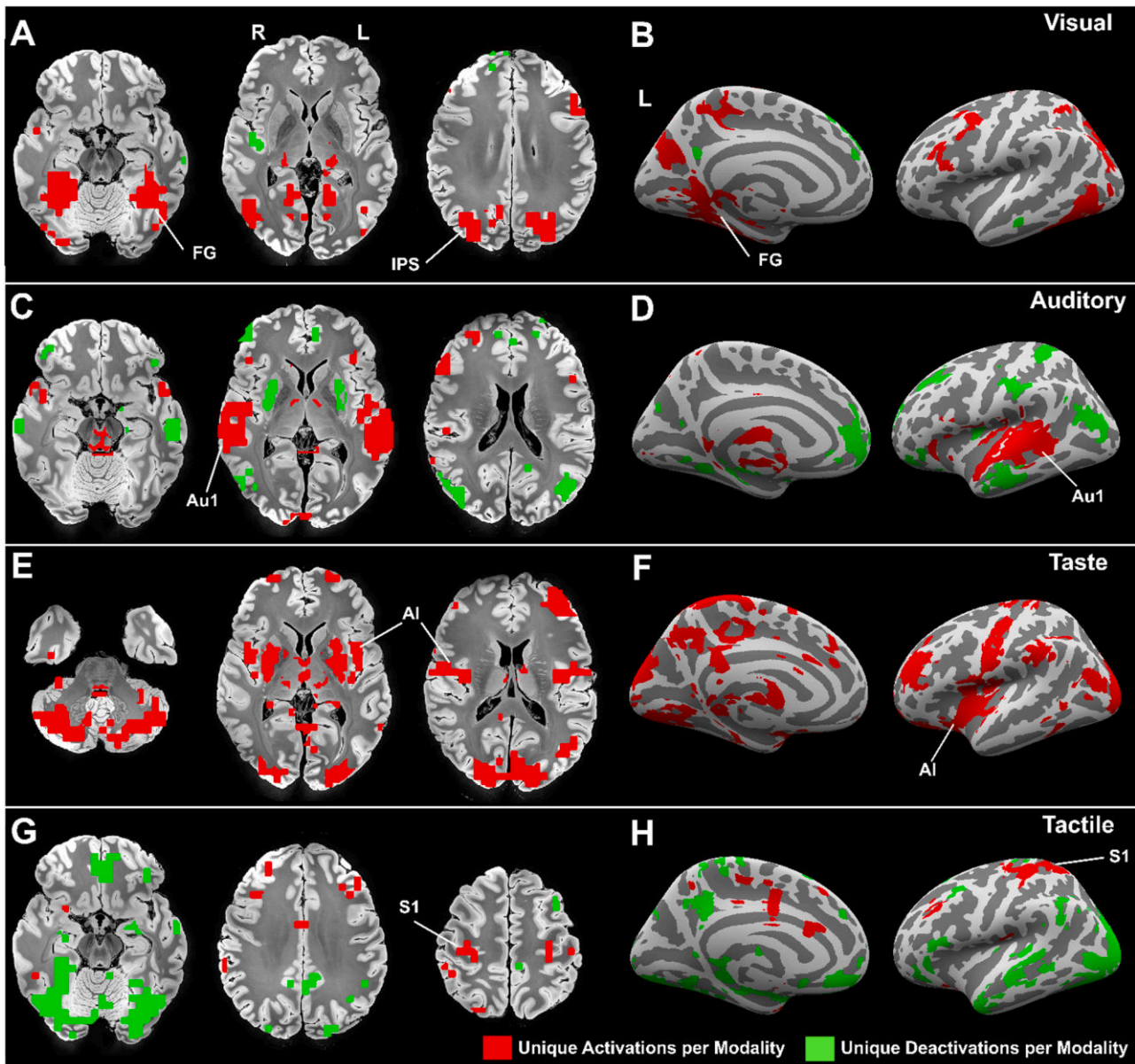


Fig. 5. Unique cortical activations (increases) and deactivations (decreases) for each of the four sensory modalities (vision, audition, taste, and touch) observed four seconds after block/event onset. Exclusive disjunction analysis identified statistically significant cortical changes present in each modality alone but in none of the other sensory modalities. (A, B) Visual disjunction analysis. (C, D) Auditory disjunction analysis. (E, F) Taste disjunction analysis. (G, H) Tactile disjunction analysis. (A, C, E, G) Axial brain slices. (B, D, F, H) Left hemisphere surface views. For additional brain slices and time points of the disjunction analyses for each modality please see Supplementary Presentation S4. Fusiform gyrus (FG), intraparietal sulcus (IPS), primary auditory cortex (Au1), anterior insula (AI), primary somatosensory cortex (S1). Same data and participants as in Fig. 1.

Discussion

We identified a shared subcortical arousal network across four sensory modalities – vision, audition, taste, and touch. The regions belonging to this network showed an early transient pulse of fMRI increases across 11 tasks within four seconds from the onset of task blocks and individual events. These increases were centered mainly on the MRF and thalamic intralaminar CL, structures pivotal for arousal and attention modulation. The time courses of percent change BOLD signals in the MRF and CL demonstrated a shared significant transient increase within four seconds from the stimulus onset. Besides CL, other nearby central thalamic nuclei overlapped with the observed increases, including, mediodorsal, ventrolateral, centromedian, and ventral medial nuclei. In addition to the identified subcortical network, a shared cortical network was activated at the same time frame in regions important for signal detection, attentional salience and top-down control such as the visual cortex, anterior insula, anterior cingulate/supplementary motor area, anterior inferior parietal lobule, superior parietal lobule, medial parietal cortex, and middle frontal gyrus. At the same time frame (four seconds from stimulus onset), less consistent increases and decreases were observed in multiple arousal and/or attention-related subcortical areas in the pons, midbrain, hypothalamus, basal forebrain, basal ganglia, and amygdala. Cortically, less consistent increases were observed in several regions such as the opercular part of the inferior frontal gyrus associated with attention control, and decreases were observed in the default mode network. Collectively, these observations provide new insights into brain mechanisms of arousal and attention irrespective of sensory modality, presented stimuli, or task demands and could lead to improved targeted therapies for disorders of arousal, attention and consciousness.

Several models of attention suggested a potential role of subcortical networks in attention modulation (Mesulam, 1981; Mohanty et al., 2008; Posner and Rothbart, 2007; Posner et al., 2006), however, previous studies have mainly focused on the role of cortical large-scale networks in top-down and bottom-up attention regulation (Corbetta and Shulman, 2002; Dosenbach et al., 2008; Fortenbaugh et al., 2017; Helfrich et al., 2019). Meanwhile, subcortical arousal networks have been mainly investigated for their involvement in controlling sustained changes of attention and state such as sleep-wake cycles (Steriade and McCarley, 2010; Edlow et al., 2024; Saper et al., 2010). Recently, the role of these subcortical networks in dynamic modulation of attention has been increasingly recognized. Previous studies suggested that arousal systems in the thalamus, upper brainstem and basal forebrain may contribute to dynamic modulation of attention and conscious perception (Sarter and Lustig, 2020; R Li et al., 2021; Schiff et al., 2013; Raver and Lin, 2015; Kinomura et al., 1996; Kronemer et al., 2022). This is further supported by lesion studies in the brainstem and thalamus identifying a key role of these regions in conscious perception and attention modulation (Parvizi and Damasio, 2003; Bogen, 1995). Although findings of several recent studies highlighted the involvement of some subcortical structures in dynamic attention control (Kronemer et al., 2022; Levinson et al., 2021), the potential role of subcortical networks in modulating attention across sensory modalities has not been investigated.

An early bilateral pulse of increases was observed within the midbrain and central thalamus within four seconds from the stimulus onset. Notably, this observation is very early given the relatively low temporal resolution of fMRI, but represents the earliest time at which the rising phase of these increases reach statistical significance, whereas the peak occurs 1–2 s later. The midbrain and central thalamic increases were common across the four sensory modalities, including vision, audition, taste, and touch. This may reflect the common role of these subcortical regions in attention modulation irrespective of the sensory modality or the specific tasks/stimuli presented to the participants. Previous studies on healthy participants and patients with impaired consciousness suggested that the MRF and central thalamus are key subcortical structures in the modulation of attention (Edlow et al., 2012;

Schiff, 2008; Schiff and Plum, 2000; R Li et al., 2019; Nagai et al., 2004; Van der Werf et al., 2002; Yanaka et al., 2010). Additionally, deep brain stimulation studies in human and animal models showed that stimulation of the central thalamus significantly improves arousal and restores consciousness (Arnts et al., 2024; Redinbaugh et al., 2020; Tasserie et al., 2022; Xu et al., 2020; ND Schiff et al., 2007; Martin et al., 2021). The early bilateral pulse of increases we identified within the MRF and central thalamus aligns with the findings from previous intracranial EEG and fMRI studies that investigated the role of these regions in conscious perception and dynamic modulation of attention across visual tasks requiring varying degrees of attention (R Li et al., 2021; Kronemer et al., 2022). Furthermore, our findings are consistent with a seminal positron emission tomography study that reported early cerebral blood flow increases in MRF and intralaminar thalamus while participants performed an attention-demanding reaction-time task (S S Kinomura et al., 1996).

Several neurotransmitters play an important role in attention and/or arousal modulation, including acetylcholine, glutamate, dopamine, noradrenaline, histamine, and orexin (Burk et al., 2018; Thiele and Bellgrove, 2018; Motelow and Blumenfeld, 2014; Mather, 2020). The current study identified various subcortical regions associated with attention modulation, each predominantly utilizing one or more of these neurotransmitters. Among the identified regions, pontine nucleus oralis, midbrain reticular formation, and central thalamus, primarily employ glutamate for attention control (Edlow et al., 2012; Motelow and Blumenfeld, 2014; Blumenfeld, 2015; Jones, 2020; Parvizi and Damasio, 2001; Shin et al., 2023). Other subcortical structures that we visualized with some involvement at early times, such as the parabrachial complex, pedunculopontine tegmental nucleus, and nucleus basalis utilize primarily acetylcholine, along with glutamate and GABA (Motelow and Blumenfeld, 2014; Blumenfeld, 2015; Blumenfeld, 2021). Meanwhile, the locus coeruleus, ventral tegmental area, and dorsal raphe use primarily noradrenaline (Mazancieux et al., 2023; Ross and Van Bockstaele, 2021), dopamine (Morales and Margolis, 2017), and serotonin (Blumenfeld, 2021; A Li et al., 2021), respectively, although each contain other neurotransmitters as well. Furthermore, the posterior hypothalamus including the tuberomammillary nucleus and the lateral hypothalamus are recognized for their roles in releasing histamine and orexin, respectively, to modulate arousal (Saper et al., 2010; Mather, 2020; Anacleit et al., 2009; Saper, 2006). Additional subcortical structures showed significant changes with respect to baseline across some sensory modalities including the superior colliculi, caudate, putamen, globus pallidus, nucleus accumbens, and amygdala. Previous studies indicated that the amygdala plays key roles in attention, arousal, and decision making (Pessoa, 2011). The superior colliculus is mainly known for its role in stimulus detection and modulation of spatial attention (Bollimunta et al., 2018; Asadollahi and Knudsen, 2016; Knudsen, 2011; Mysore and Knudsen, 2013; Wang et al., 2022), and is associated with early transient BOLD increases, consistent with its role in sensory processing and attentional shifts (Wall et al., 2009). Basal ganglia structures including the caudate, putamen, globus pallidus, and nucleus accumbens were found to control sleep-wake transitions (Lazarus et al., 2013) and play a role in recovery of consciousness after a brain injury (Edlow et al., 2021; Schiff, 2010). Although we identified BOLD decreases in basal ganglia for some modalities, these decreases do not necessarily reflect decreases in neural activity (Cerri et al., 2024; Mishra et al., 2011).

In the cortex, we identified a shared network that includes regions involved in event detection, bottom-up attentional salience, top-down attentional control, conscious perception, and motor preparation (R Li et al., 2021; Kronemer et al., 2022; Barry et al., 2012; Corbetta and Shulman, 2002; V. V Menon and Uddin, 2010; Seeley et al., 2007; Barcelo, 2003; Kincade et al., 2005). The identified regions included anterior insula and anterior cingulate/supplementary motor area which are key structures in the salience network as well as additional regions belonging to the attention and executive control networks, including regions of the parietal lobe and lateral frontal cortex (R Li et al., 2021;

Kronemer et al., 2022; Barry et al., 2012; Corbetta and Shulman, 2002; V. V. Menon and Uddin, 2010; Seeley et al., 2007). Interestingly, consistent early cortical increases across modalities also included the primary visual cortex, which may speak to the potential cross-modal function of some primary cortical regions in sensory processing (Teichert and Bolz, 2018). Less consistent increases were observed in the opercular part of the inferior frontal gyrus, known to play a role in attention control (Cazzoli et al., 2021; Chong et al., 2008; Hampshire et al., 2010), and less consistent decreases were observed in well-known default mode areas, including ventromedial frontal cortex, precuneus, and the posterior inferior parietal lobule (R Li et al., 2021; Kronemer et al., 2022; Herman et al., 2019; J Li et al., 2019; Raichle and Snyder, 2007; Singh and Fawcett, 2008).

Our findings support a data-driven hypothesis we introduced previously to describe the sequence of neural mechanisms required to produce conscious perceptual awareness of external sensory stimuli (Blumenfeld, 2023). In particular, the transient pulse of activation in subcortical arousal systems observed across sensory modalities in the current study fits in this framework. We hypothesize that for a sensory stimulus to be consciously perceived, it has to be first detected by the primary cortex and other cortical and subcortical signal detection circuits. Next, a dynamic transient pulse of activity in subcortical and cortical arousal systems modulates attention and facilitates subsequent widespread signal processing necessary for conscious perception. Then, potentially competing activity in the default mode network is switched off. Finally, a broad wave of hierarchical processing progresses through association cortical areas to fully process the event before it is encoded in memory systems. Our present findings strengthen this hypothesis (Blumenfeld, 2023) by identifying a highly consistent transient pulse of increased fMRI activity in midbrain and central thalamus shared across visual, tactile, auditory and taste stimuli, associated with transitions of attention in tasks requiring sensory perception.

The disjunction analysis helped to validate our approach by showing cortical and subcortical regions that are well-known to be associated with each sensory modality. For instance, visual tasks showed unique activations in lateral geniculate nucleus, pulvinar, fusiform gyrus and the intraparietal sulcus (Gupta et al., 2024; Singh-Curry and Husain, 2009), while auditory tasks showed unique activations in superior olivary nuclear complex, inferior colliculus, medial geniculate nucleus, and primary auditory cortex (Peterson et al., 2024). Unique activations for taste included the nucleus solitarius, ventral posterior medial nucleus, amygdala, and anterior insular cortex (Avery et al., 2020; Kawakami et al., 2015). Additionally, unique increases were observed for touch in the caudate nucleus and primary somatosensory cortex (Kitada et al., 2019; Yeon et al., 2017). Unique decreases in different parts of the putamen were found in audition and touch. Previous studies have shown that the putamen is involved in attentive processing of auditory or tactile stimuli, but with increased BOLD activity (Opitz et al., 2005; Peller et al., 2006; Halder et al., 2019). Thus, the decreases observed in the current study need to be further investigated (Mishra et al., 2011).

Our study has several limitations that should be addressed in future work. Techniques have been proposed to improve inter-subject subcortical co-registration, but are so far not widely used (Balakrishnan et al., 2019; Cheng et al., 2020). These approaches typically require high computational costs, rendering their application impractical in our present study due to the substantial sample size, which exceeded 1500 participants. Because we did not use such approaches in the current study, we were cautious to avoid making strong conclusions on the voxel level, particularly if the activations/deactivations were not centered on anatomically known structures. While subcortical analyses were performed at a 2 mm isotropic voxel size, some datasets included in the study were acquired with larger voxel sizes (UCLA: 4 mm isotropic, Glasgow: 3 mm isotropic, Tactile: 2.1 mm isotropic). This variation in spatial resolution could influence the precision of the results, especially in smaller subcortical regions, where lower resolution may limit the ability to accurately delineate fine

structures. Given the variability in the duration of baseline periods prior to stimulus onset across tasks (see Table 1), we employed a relatively short baseline (6 s) for our statistical analysis to minimize the effect of any preceding stimuli on our results. This potential confound is particularly relevant for the tactile task, where the relatively short baseline period (4–8 s) could potentially be contaminated by the preceding task block, and the TR of 3 s may also reduce confidence in the temporal resolution for the tactile data. To mitigate this concern, we used a relatively short baseline period of 6 s to reduce these potential confounds, however in future studies longer baseline periods would likely provide a more robust estimate of the pre-stimulus activity. Although we included large sample sizes to identify the shared subcortical and cortical networks, the analyzed datasets were not balanced across sensory modalities due to the limited availability of tasks from certain sensory modalities such as taste and touch. No olfaction tasks suiting our analysis purposes were available. Future studies should aim to balance the sample sizes across sensory modalities, and should include more taste and tactile tasks if available. Inclusion of olfaction tasks is an important future direction, particularly because some olfactory signaling pathways bypass the thalamus. This will help to further identify the shared changes across all senses. The current study primarily focuses on investigating transient subcortical signals, rather than sustained changes. Previous studies have investigated sustained BOLD changes in block design tasks in single sensory modalities (R Li et al., 2021; Uludag, 2008; NUF Dosenbach et al., 2007; MD MD Fox et al., 2005). However, future studies in multiple modalities could explore longer time scales to examine sustained effects, which may provide additional insights into the dynamics of BOLD responses over extended periods across sensory modalities. Although fMRI provides comprehensive anatomical mapping of cortical and subcortical structures not available with more spatially limited human electrophysiological methods, it has lower temporal resolution, and therefore may provide limited information about the sequence of activations/deactivations within the observed networks. Further investigation of these networks could be performed in animal models through direct electrophysiological recordings, or in human studies with availability of subcortical depth electrodes (Kronemer et al., 2022) to identify the temporal dynamics of these networks. In addition, regions that are common to some but not all sensory modalities need to be investigated further to identify why they are specific to certain sensory modalities but not others.

In summary, although previous work in conscious perception and attention modulation has recognized the regions we found, prior studies were conducted predominantly in individual sensory modalities. Our approach of analyzing different tasks spanning multiple sensory modalities and with large sample size, enabled us to identify changes independent of the task design, demands or stimulus type. We found that the most consistent subcortical change associated with transitions in attention was a transient increase in activity in the MRF and central thalamus. These subcortical changes were accompanied by consistent increases in activity in cortical detection, arousal and salience networks, as well as by less consistent changes in multiple other subcortical and cortical regions. Further investigation of the shared subcortical arousal systems participating across sensory modalities could lead to improved targeted therapies for disorders of arousal, attention and consciousness (ND ND Schiff et al., 2007; Schiff et al., 2023; Kundishora et al., 2017; Gummadavelli et al., 2015) and a better understanding of the complex spatiotemporal mechanisms of normal brain function.

Code availability

Analysis codes for this study are publicly available at: https://github.com/BlumenfeldLab/Khalaf-et-al_2025

CRediT authorship contribution statement

Aya Khalaf: Writing – review & editing, Writing – original draft,

Visualization, Validation, Project administration, Methodology, Investigation, Formal analysis, Conceptualization. **Erick Lopez:** Writing – review & editing, Formal analysis. **Jian Li:** Writing – review & editing, Methodology. **Andreas Horn:** Writing – review & editing, Methodology. **Brian L. Edlow:** Writing – review & editing, Methodology. **Hal Blumenfeld:** Writing – review & editing, Supervision, Resources, Project administration, Methodology, Funding acquisition, Formal analysis, Conceptualization.

Declaration of competing interest

The authors declare that they have no known competing financial interests or personal relationships that could have appeared to influence the work reported in this paper.

Acknowledgements

This work was supported by NIH R01 NS134655 (to H.B.), the Mark Loughridge and Michele Williams Foundation, and the Betsy and Jonathan Blattmachr family. A.H. was supported by the German Research Foundation (Deutsche Forschungsgemeinschaft, 424778381 – TRR 295), Deutsches Zentrum für Luft- und Raumfahrt (DynaSti grant within the EU Joint Programme Neurodegenerative Disease Research, JPND), the National Institutes of Health (R01MH130666, 1R01NS127892–01, 2R01 MH113929 & UM1NS132358) as well as the New Venture Fund (FFOR Seed Grant). A.H. reports lecture fees for Boston Scientific and is a consultant for FxNeuromodulation and Abbott.

Supplementary materials

Supplementary material associated with this article can be found, in the online version, at [doi:10.1016/j.neuroimage.2025.121224](https://doi.org/10.1016/j.neuroimage.2025.121224).

Data availability

Datasets included in this study are publicly available through the OpenNeuro and Human Connectome Project websites.

References

- Anaclet, C., Parmentier, R., Ouk, K., et al., 2009. Orexin/hypocretin and histamine: distinct roles in the control of wakefulness demonstrated using knock-out mouse models. *J. Neurosci.* 29, 14423–14438.
- Angsturm, P., Hense, K., Rosengarth, K., et al., 2024. Attenuation of the BOLD fMRI signal and changes in functional connectivity affecting the whole brain in presence of brain metastasis. *Cancers* 16.
- Arnts, H., Tewarie, P., van Erp, W., et al., 2024. Deep brain stimulation of the central thalamus restores arousal and motivation in a zolpidem-responsive patient with akinetic mutism after severe brain injury. *Sci. Rep.* 14, 2950.
- Asadollahi, A., Knudsen, E.L., 2016. Spatially precise visual gain control mediated by a cholinergic circuit in the midbrain attention network. *Nat. Commun.* 7, 13472.
- Avery, J.A., Liu, A.G., Ingeholm, J.E., Riddell, C.D., Gotts, S.J., Martin, A., 2020. Taste quality representation in the Human brain. *J. Neurosci.* 40, 1042–1052.
- Bai, X., Vestal, M., Berman, R., et al., 2010. Dynamic time course of typical childhood absence seizures: EEG, behavior, and functional magnetic resonance imaging. *J. Neurosci.* 30, 5884–5893.
- Bai, X.X., Vestal, M., Berman, R., et al., 2010. Dynamic time course of typical childhood absence seizures: EEG, behavior, and functional magnetic resonance imaging. *J. Neurosci.* 30, 5884–5893.
- Balakrishnan, G., Zhao, A., Sabuncu, M.R., Guttig, J., Dalca, A.V., 2019. VoxelMorph: a learning framework for deformable medical image registration. *IEEE Trans. Med. Imaging*.
- Bansal, R., Peterson, B.S., 2018. Cluster-level statistical inference in fMRI datasets: the unexpected behavior of random fields in high dimensions. *Magn. Reson. Imaging* 49, 101–115.
- Barcelo, F., 2003. The Madrid card sorting test (MCST): a task switching paradigm to study executive attention with event-related potentials. *Brain Res. Brain Res. Protocols* 11, 27–37.
- Barch, D.M., Burgess, G.C., Harms, M.P., et al., 2013. Function in the human connectome: task-fMRI and individual differences in behavior. *Neuroimage* 80, 169–189.
- Barry, R.J., Steiner, G.Z., De Blasio, F.M., 2012. Event-related EEG time-frequency analysis and the Orienting reflex to auditory stimuli. *Psychophysiology* 49, 744–755.
- Bijsterbosch, J., Smith, S.M., Beckmann, C., 2017. An Introduction to Resting State fMRI Functional Connectivity. Oxford University Press.
- Binder, J.R., Gross, W.L., Allendorfer, J.B., et al., 2011. Mapping anterior temporal lobe language areas with fMRI: a multicenter normative study. *Neuroimage* 54, 1465–1475.
- Eds: Blumenfeld, H., 2015. Neuroanatomical basis of consciousness. In: Gosseries, O., Laureys, S. (Eds.), *The Neurology of Consciousness*, 2nd Edition. G Tononi Elsevier, Ltd. Eds:Ch 1.
- Blumenfeld, H., 2021. Arousal and consciousness in focal seizures. *Epilepsy Curr.* 21, 353–359.
- Blumenfeld, H., 2023. Brain mechanisms of conscious awareness: detect, pulse, switch, and wave. *Neuroscientist* 29, 9–18.
- Bogen, J.E., 1995. On the neurophysiology of consciousness: I. An overview. *Conscious. Cogn.* 4, 52–62.
- Bollimunta, A., Bogadhi, A.R., Krauzlis, R.J., 2018. Comparing frontal eye field and superior colliculus contributions to covert spatial attention. *Nat. Commun.* 9, 3553.
- Buckner, R.L., Bandettini, P.A., O'Craven, K.M., et al., 1996. Detection of cortical activation during averaged single trials of a cognitive task using functional magnetic resonance imaging. *Proc. Natl. Acad. Sci. USA* 93, 14878–14883.
- Buckner, R.L., Krienen, F.M., Castellanos, A., Diaz, J.C., Yeo, B.T.T., 2011. The organization of the human cerebellum estimated by intrinsic functional connectivity. *J. Neurophysiol.* 106, 2322–2345.
- Burk, J.A., Blumenthal, S.A., Maness, E.B., 2018. Neuropharmacology of attention. *Eur. J. Pharmacol.* 835, 162–168.
- Caceres, A., Hall, D.L., Zelaya, F.O., Williams, S.C.R., Mehta, M.A., 2009. Measuring fMRI reliability with the intra-class correlation coefficient. *Neuroimage* 45, 758–768.
- Candemir, C., 2023. Spatial smoothing effect on group-level functional connectivity during resting and task-based fMRI. *Sensors-Basel* 23.
- Castelli, F., Happe, F., Frith, U., Frith, C., 2000. Movement and mind: A functional imaging study of perception and interpretation of complex intentional movement patterns. *Neuroimage* 12, 314–325.
- Cazzoli, D., Kaufmann, B.C., Paladini, R.M., Muri, R.M., Nef, T., Nyffeler, T., 2021. Anterior insula and inferior frontal gyrus: where ventral and dorsal visual attention systems meet. *Brain Commun.* 3, fcaa220.
- Cerri, D.H., Albaugh, D.L., Walton, L.R., et al., 2024. Distinct neurochemical influences on fMRI response polarity in the striatum. *Nat. Commun.* 15, 1916.
- Chee, M.W.L., Venkatraman, V., Westphal, C., Siong, S.C., 2003. Comparison of block and event-related fMRI designs in evaluating the word-frequency effect. *Hum. Brain Mapp.* 18, 186–193.
- Cheng, J., Dalca, A.V., Fischl, B., Zollei, L., 2020. Alzheimer's Disease neuroimaging I. Cortical surface registration using unsupervised learning. *Neuroimage* 221, 117161.
- Chong, T.T., Williams, M.A., Cunnington, R., Mattingley, J.B., 2008. Selective attention modulates inferior frontal gyrus activity during action observation. *Neuroimage* 40, 298–307.
- Corbetta, M., Shulman, G.L., 2002. Control of goal-directed and stimulus-driven attention in the brain. *Nat. Rev. Neurosci.* 3, 201–215.
- Czarnecka, M., Raczky, K., Szewczyk, J., et al., 2023. Overlapping but separate number representations in the intraparietal sulcus-probing format- and modality-independence in sighted Braille readers. *Cortex* 162, 65–80.
- Dalenberg, J.R., Patel, B.P., Denis, R., et al., 2020. Short-term consumption of sucralose with, but not without, carbohydrate impairs neural and metabolic sensitivity to sugar in humans. *Cell Metab.* 31, 493. –+.
- Dehaene, S., 2014. *Consciousness and the brain: Deciphering how the Brain Codes Our Thoughts*. Viking Adult, New York.
- Delgado, M.R., Nystrom, L.E., Fissell, C., Noll, D.C., Fiez, J.A., 2000. Tracking the hemodynamic responses to reward and punishment in the striatum. *J. Neurophysiol.* 84, 3072–3077.
- Dosenbach, N.U., Fair, D.A., Miezin, F.M., et al., 2007. Distinct brain networks for adaptive and stable task control in humans. *Proc. Natl. Acad. Sci. USA* 104, 11073–11078.
- Dosenbach, N.U.F., Fair, D.A., Miezin, F.M., et al., 2007. Distinct brain networks for adaptive and stable task control in humans. *Proc. Natl. Acad. Sci. USA* 104, 11073–11078.
- Dosenbach, N.U., Fair, D.A., Cohen, A.L., Schlaggar, B.L., Petersen, S.E., 2008. A dual-networks architecture of top-down control. *Trends Cogn. Sci. (Regul. Ed.)* 12, 99–105.
- Drobyshevsky, A., Baumann, S.B., Schneider, W., 2006. A rapid fMRI task battery for mapping of visual, motor, cognitive, and emotional function. *Neuroimage* 31, 732–744.
- Edlow, B.L., Takahashi, E., Wu, O.N., et al., 2012. Neuroanatomic connectivity of the Human ascending arousal system critical to consciousness and its disorders. *J. Neuropath. Exp. Neurol.* 71, 531–546.
- Edlow, B.L., Mareyam, A., Horn, A., et al., 2019. Tesla MRI of the human brain at 100 μ m resolution. *Sci. Data* 6.
- Edlow, B.L., Claassen, J., Schiff, N.D., Greer, D.M., 2021. Recovery from disorders of consciousness: mechanisms, prognosis and emerging therapies. *Nat. Rev. Neurol.* 17, 135–156.
- Edlow, B.L., Olchanyi, M., Freeman, H.J., et al., 2024. Multimodal MRI reveals brainstem connections that sustain wakefulness in human consciousness. *Sci. Transl. Med.* 16, eadj4303.
- Fortenbaugh, F.C., DeGutis, J., Esterman, M., 2017. Recent theoretical, neural, and clinical advances in sustained attention research. *Ann. NY Acad. Sci.* 1396, 70–91.

- Fox, M.D., Snyder, A.Z., Vincent, J.L., Corbetta, M., Van Essen, D.C., Raichle, M.E., 2005. The human brain is intrinsically organized into dynamic, anticorrelated functional networks. *Proc. Natl. Acad. Sci. USA* 102, 9673–9678.
- Fox, M.D., Snyder, A.Z., Barch, D.M., Gusnard, D.A., Raichle, M.E., 2005. Transient BOLD responses at block transitions. *Neuroimage* 28, 956–966.
- Fox, M.D., Snyder, A.Z., Barch, D.M., Gusnard, D.A., Raichle, M.E., 2005. Transient BOLD responses at block transitions. *Neuroimage* 28, 956–966.
- Gläscher, J., 2009. Visualization of group inference data in functional neuroimaging. *Neuroinformatics* 7, 73–82.
- Glasser, M.F., Sotiropoulos, S.N., Wilson, J.A., et al., 2013. The minimal preprocessing pipelines for the Human Connectome Project. *Neuroimage* 80, 105–124.
- Gonzalez-Castillo, J., Saad, Z.S., Handwerker, D.A., Inati, S.J., Brenowitz, N., Bandettini, P.A., 2012. Whole-brain, time-locked activation with simple tasks revealed using massive averaging and model-free analysis. *Proc. Natl. Acad. Sci. USA* 109, 5487–5492.
- Grill-Spector, K., Knouf, N., Kanwisher, N., 2004. The fusiform face area subserves face perception, not generic within-category identification. *Nat. Neurosci.* 7, 555–562.
- Groppe, D.M., Urbach, T.P., Kutas, M., 2011. Mass univariate analysis of event-related brain potentials/fields I: a critical tutorial review. *Psychophysiology* 48, 1711–1725.
- Gummadavelli, A., Kundishora, A.J., Willie, J.T., et al., 2015. Improving level of consciousness in epilepsy with neurostimulation. *Neurosurg. Focus* 38 (6), E10.
- Guo, J.N., Kim, R., Chen, Y., et al., 2016. Impaired consciousness in patients with absence seizures investigated by functional MRI, EEG, and behavioural measures: a cross-sectional study. *Lancet Neurol.* 15, 1336–1345.
- Gupta, M., Ireland, A.C., Neuroanatomy, Bordonì B., 2024. Visual Pathway. *StatPearls*. Treasure Island (FL) ineligible companies. Disclosure: ashley Ireland declares no relevant financial relationships with ineligible companies. Disclosure.
- Halder, S., Leinfelder, T., Schulz, S.M., Kubler, A., 2019. Neural mechanisms of training an auditory event-related potential task in a brain-computer interface context. *Hum. Brain Mapp.* 40, 2399–2412.
- Hampshire, A., Chamberlain, S.R., Monti, M.M., Duncan, J., Owen, A.M., 2010. The role of the right inferior frontal gyrus: inhibition and attentional control. *Neuroimage* 50, 1313–1319.
- Handwerker, D., Ollinger, J., D'Esposito, M., 2004. Variation of BOLD hemodynamic responses across subjects and brain regions and their effects on statistical analyses. *Neuroimage* 21, 1639–1651.
- Helfrich, R.F., Breska, A., Knight, R.T., 2019. Neural entrainment and network resonance in support of top-down guided attention. *Curr. Opin. Psychol.* 29, 82–89.
- Herman, W.X., Smith, R.E., Kronemer, S.I., et al., 2019. A switch and wave of neuronal activity in the cerebral cortex during the first second of conscious perception. *Cereb. Cortex* 29, 461–474.
- Janacek, K., Evans, T.M., Kiss, M., Shah, L., Blumenfeld, H., Ullman, M.T., 2022. Subcortical cognition: the fruit below the rind. *Annu. Rev. Neurosci.* 45, 361–386.
- Jones, B.E., 2020. Arousal and sleep circuits. *Neuropsychopharmacology* 45, 6–20.
- Kanwisher, N., McDermott, J., Chun, M.M., 1997. The fusiform face area: a module in human extrastriate cortex specialized for face perception. *J. Neurosci.* 17, 4302–4311.
- Kanwisher, N., Tong, F., Nakayama, K., 1998. The effect of face inversion on the human fusiform face area. *Cognition* 68, B1–11.
- Kawakami, S., Sato, H., Sasaki, A.T., et al., 2015. The brain mechanisms underlying the perception of pungent taste of capsaicin and the subsequent autonomic responses. *Front. Hum. Neurosci.* 9, 720.
- Kinade, J.M., Abrams, R.A., Astafiev, S.V., Shulman, G.L., Corbetta, M., 2005. An event-related functional magnetic resonance imaging study of voluntary and stimulus-driven orienting of attention. *J. Neurosci.* 25, 4593–4604.
- Kinomura, S., Larsson, J., Gulyas, B., Roland, P.E., 1996. Activation by attention of the human reticular formation and thalamic intralaminar nuclei. *Science* 271, 512–515.
- Kinomura, S., Larsson, J., Gulyas, B., Roland, P.E., 1996. Activation by attention of the human reticular formation and thalamic intralaminar nuclei. *Science* 271, 512.
- Kitada, R., Doizaki, R., Kwon, J., et al., 2019. Brain networks underlying tactile softness perception: a functional magnetic resonance imaging study. *Neuroimage* 197, 156–166.
- Knudsen, E.I., 2011. Control from below: the role of a midbrain network in spatial attention. *Eur. J. Neurosci.* 33, 1961–1972.
- Koch, C., Massimini, M., Boly, M., Tononi, G., 2016. Neural correlates of consciousness: progress and problems. *Nat. Rev. Neurosci.* 17, 307–321.
- Kronemer, S.I., Aksen, M., Ding, J.Z., et al., 2022. Human visual consciousness involves large scale cortical and subcortical networks independent of task report and eye movement activity. *Nat. Commun.* 13, 7342.
- Kundishora, A.J., Gummadavelli, A., Ma, C., et al., 2017. Restoring conscious arousal during focal limbic seizures with deep brain stimulation. *Cereb. Cortex* 27, 1964–1975.
- Kwon, H., Kronemer, S.I., Kl, Christison-Lagay, et al., 2021. Early cortical signals in visual stimulus detection. *Neuroimage* 244, 118608.
- Lazarus, M., Chen, J.F., Urade, Y., Huang, Z.L., 2013. Role of the basal ganglia in the control of sleep and wakefulness. *Curr. Opin. Neurobiol.* 23, 780–785.
- Levinson, M., Podvalny, E., Baete, S.H., He, B.J., 2021. Cortical and subcortical signatures of conscious object recognition. *Nat. Commun.* 12, 2930.
- Li, R., Hu, C., Wang, L., et al., 2019. Disruption of functional connectivity among subcortical arousal system and cortical networks in temporal lobe epilepsy. *Brain Imaging Behav.* 1–10.
- Li, J., Kronemer, S.I., Herman, W.X., et al., 2019. Default mode and visual network activity in an attention task: direct measurement with intracranial EEG. *Neuroimage* 201, 116003.
- Li, R., Ryu, J.H., Vincent, P., et al., 2021. The pulse: transient fMRI signal increases in subcortical arousal systems during transitions in attention. *Neuroimage* 232, 117873.
- Li, A., Li, R., Ouyang, P.R., et al., 2021. Dorsal raphe serotonergic neurons promote arousal from isoflurane anesthesia. *CNS. Neurosci. Ther.* 27, 941–950.
- Maisog, J.M., Chmielewska, J., 1998. An efficient method for correcting the edge artifact due to smoothing. *Hum. Brain Mapp.* 6, 128–136.
- Maris, E., Oostenveld, R., 2007. Nonparametric statistical testing of EEG- and MEG-data. *J. Neurosci. Methods* 164, 177–190.
- Martin, R.A., Cukiert, A., Blumenfeld, H., 2021. Short-term changes in cortical physiological arousal measured by electroencephalography during thalamic centromedian deep brain stimulation. *Epilepsia* 62, 2604–2614.
- Mather, M., 2020. How arousal-related neurotransmitter systems compensate for age-related decline. In: Thomas, A., Gutchess, A. (Eds.), *The Cambridge Handbook of Cognitive Aging: A Life Course Perspective*. Cambridge University Press, pp. 101–120.
- Mazancieux, A., Mauconduit, F., Amadon, A., Willem de Gee, J., Donner, T.H., Meyniel, F., 2023. Brainstem fMRI signaling of surprise across different types of deviant stimuli. *Cell Rep.* 42, 113405.
- McCafferty, C., Gruenbaum, B.F., Tung, R., et al., 2023. Decreased but diverse activity of cortical and thalamic neurons in consciousness-impairing rodent absence seizures. *Nat. Commun.* 14, 117.
- Menon, V., Uddin, L.Q., 2010. Saliency, switching, attention and control: a network model of insula function. *Brain Struct. Funct.* 214, 655–667.
- Menon, V., Uddin, L.Q., 2010. Saliency, switching, attention and control: a network model of insula function. *Brain Struct. Funct.* 214, 655–667.
- Mesulam, M.M., 1981. A cortical network for directed attention and unilateral neglect. *Ann. Neurol.* 10, 309–325.
- Mikl, M., Marecek, R., Hlustik, P., et al., 2008. Effects of spatial smoothing on fMRI group inferences. *Magn. Reson. Imaging* 26, 490–503.
- Mishra, A.M., Ellens, D.J., Schridde, U., et al., 2011. Where fMRI and electrophysiology agree to disagree: corticothalamic and striatal activity patterns in the WAG/Rij rat. *J. Neurosci.* 31, 15053–15064.
- Mohanty, A., Gitelman, D.R., Small, D.M., Mesulam, M.M., 2008. The spatial attention network interacts with limbic and monoaminergic systems to modulate motivation-induced attention shifts. *Cereb. Cortex* 18, 2604–2613.
- Morales, M., Margolis, E.B., 2017. Ventral tegmental area: cellular heterogeneity, connectivity and behaviour. *Nat. Rev. Neurosci.* 18, 73–85.
- Motelow, J., Blumenfeld, H., 2014. Consciousness and subcortical arousal systems. In: Faingold, C.L., Blumenfeld, H. (Eds.), *Neuronal Networks in Brain Function, CNS Disorders, and Therapeutics*. Elsevier, pp. 277–298. Ch 21.
- Mysore, S.P., Knudsen, E.I., 2013. A shared inhibitory circuit for both exogenous and endogenous control of stimulus selection. *Nat. Neurosci.* 16, 473–478.
- Nagai, Y., Critchley, H.D., Featherstone, E., Fenwick, P.B., Trimble, M.R., Dolan, R.J., 2004. Brain activity relating to the contingent negative variation: an fMRI investigation. *Neuroimage* 21, 1232–1241.
- Neudorfer, C., Germann, J., Elias, G.J.B., Gramer, R., Boutet, A., Lozano, A.M., 2020. A high-resolution magnetic resonance imaging atlas of the human hypothalamic region. *Sci. Data* 7.
- Niemann, K., Mennicken, V.R., Jeanmonod, D., Morel, A., 2000. The morel stereotactic atlas of the human thalamus: atlas-to-MR registration of internally consistent Canonical Model. *Neuroimage* 12, 601–616.
- Opitz, B., Schroger, E., von Cramon, D.Y., 2005. Sensory and cognitive mechanisms for preattentive change detection in auditory cortex. *Eur. J. Neurosci.* 21, 531–535.
- Paret, C., Kluetsch, R., Ruf, M., et al., 2014. Transient and sustained BOLD signal time courses affect the detection of emotion-related brain activation in fMRI. *Neuroimage* 103, 522–532.
- Parvizi, J., Damasio, A., 2001. Consciousness and the brainstem. *Cognition* 79, 135–159.
- Parvizi, J., Damasio, A.R., 2003. Neuroanatomical correlates of brainstem coma. *Brain* 126, 1524–1536.
- Peller, M., Zeuner, K.E., Munchau, A., et al., 2006. The basal ganglia are hyperactive during the discrimination of tactile stimuli in writer's cramp. *Brain* 129, 2697–2708.
- Pernet, C.R., McAleer, P., Latinus, M., et al., 2015. The human voice areas: spatial organization and inter-individual variability in temporal and extra-temporal cortices. *Neuroimage* 119, 164–174.
- Pessoa, L., 2011. Emotion and cognition and the amygdala: from "what is it?" to "what's to be done?" (Reprinted from *Neuropsychologia*, vol 48, pg 3416–3429, 2010). *Neuropsychologia* 49, 681–694.
- Peterson, D.C., Reddy, V., Launico, M.V., Neuroanatomy, Hamel RN., 2024. Auditory Pathway. *StatPearls*. Treasure Island (FL) ineligible companies. Disclosure: vamsi Reddy declares no relevant financial relationships with ineligible companies. Disclosure: marjorie Launico declares no relevant financial relationships with ineligible companies. Disclosure.
- Poldrack, R.A., Congdon, E., Triplett, W., et al., 2016. A phenome-wide examination of neural and cognitive function. *Sci. Data* 3.
- Poldrack, R.A., Mumford, J.A., Nichols, T.E., 2024. *Handbook of Functional MRI Data Analysis*. Cambridge University Press.
- Posner, M.I., Rothbart, M.K., 2007. Research on attention networks as a model for the integration of psychological science. *Annu. Rev. Psychol.* 58, 1–23.
- Posner, M.I., Sheese, B.E., Odludas, Y., Tang, Y., 2006. Analyzing and shaping human attentional networks. *Neural Netw.* 19, 1422–1429.
- Power, J., KA, B., AZ, S., BL, S., SE, P., 2012. Spurious but systematic correlations in functional connectivity MRI networks arise from subject motion. *Neuroimage* 59, 2142–2154.

- Prodoeh, J., Yu, H., Little, D.M., Abraham, I., Vaillancourt, D.E., 2008. Region of interest template for the human basal ganglia: comparing EPI and standardized space approaches. *Neuroimage* 39, 956–965.
- Raichle, M.E., Snyder, A.Z., 2007. A default mode of brain function: a brief history of an evolving idea. *Neuroimage* 37, 1083–1090.
- Raver, S.M., Lin, S.C., 2015. Basal forebrain motivational salience signal enhances cortical processing and decision speed. *Front. Behav. Neurosci.* 9, 277.
- Redinbaugh, M.J., Phillips, J.M., Kambi, N.A., et al., 2020. Thalamus modulates consciousness via layer-specific control of cortex. *Neuron* 106, 66–75 e12.
- Ross, J.A., Van Bockstaele, E.J., 2021. The Locus Coeruleus- Norepinephrine system in stress and arousal: unraveling historical, current, and future perspectives. *Front. Psychiatry* 11.
- Saper, C.B., Fuller, P.M., Pedersen, N.P., Lu, J., Scammell, T.E., 2010. Sleep State switching. *Neuron* 68, 1023–1042.
- Saper, C.B., 2006. Staying awake for dinner: hypothalamic integration of sleep, feeding, and circadian rhythms. *Prog. Brain Res.* 153, 243–252.
- Sarter, M., Lustig, C., 2020. Forebrain cholinergic signaling: wired and phasic, not tonic, and causing behavior. *J. Neurosci.* 40, 712–719.
- Schiff, N.D., Plum, F., 2000. The role of arousal and "gating" systems in the neurology of impaired consciousness. *J. Clin. Neurophysiol.* 17, 438–452.
- Schiff, N.D., Giacino, J.T., Kalmar, K., et al., 2007. Behavioural improvements with thalamic stimulation after severe traumatic brain injury. *Nature* 448, 600–U610.
- Schiff, N.D., Giacino, J.T., Kalmar, K., et al., 2007. Behavioural improvements with thalamic stimulation after severe traumatic brain injury. *Nature* 448, 600–603.
- Schiff, N.D., Shah, S.A., Hudson, A.E., Nauvel, T., Kalik, S.F., Purpura, K.P., 2013. Gating of attentional effort through the central thalamus. *J. Neurophysiol.* 109, 1152–1163.
- Schiff, N.D., Giacino, J.T., Butson, C.R., et al., 2023. Thalamic deep brain stimulation in traumatic brain injury: a phase 1, randomized feasibility study. *Nat. Med.* 29, 3162–3174.
- Schiff, N.D., 2008. Central thalamic contributions to arousal regulation and neurological disorders of consciousness. *Ann. NY Acad. Sci.* 1129, 105–118.
- Schiff, N.D., 2010. Recovery of consciousness after brain injury: a mesocircuit hypothesis. *Trends. Neurosci.* 33, 1–9.
- Seeley, W.W., Menon, V., Schatzberg, A.F., et al., 2007. Dissociable intrinsic connectivity networks for salience processing and executive control. *J. Neurosci.* 27, 2349–2356.
- Setzer, B., Fultz, N.E., Gomez, D.E.P., et al., 2022. A temporal sequence of thalamic activity unfolds at transitions in behavioral arousal state. *Nat. Commun.* 13.
- Shin, A., Park, S., Shin, W., et al., 2023. A brainstem-to-mediadorsal thalamic pathway mediates sound-induced arousal from slow-wave sleep. *Curr. Biol.* 33, 875. –+.
- Shulman, G.L., Fiez, J.A., Corbetta, M., et al., 1997. Common blood flow changes across visual tasks: II. Decreases in cerebral cortex. *J. Cogn. Neurosci.* 9 (5), 648–663.
- Singh, K., Fawcett, I., 2008. Transient and linearly graded deactivation of the human default-mode network by a visual detection task. *Neuroimage* 41, 100–112.
- Singh-Curry, V., Husain, M., 2009. The functional role of the inferior parietal lobe in the dorsal and ventral stream dichotomy. *Neuropsychologia* 47, 1434–1448.
- Smith, R., Keramian, K., Christoff, K., 2007. Localizing the rostrolateral prefrontal cortex at the individual level. *Neuroimage* 36, 1387–1396.
- Smyser, C., Inder, T., Shimony, J., et al., 2010. Longitudinal analysis of neural network development in preterm infants. *Cerebral Cortex* 20, 2852–2862.
- Steriade, M.M., McCarley, R.W., 2010. *Brain Control of Wakefulness and Sleep*, 2nd ed. Springer.
- Tambini, A., Ketz, N., Davachi, L., 2010. Enhanced brain correlations during rest are related to memory for recent experiences. *Neuron* 65, 280–290.
- Tasserie, J., Uhrig, L., Sitt, J.D., et al., 2022. Deep brain stimulation of the thalamus restores signatures of consciousness in a nonhuman primate model. *Sci. Adv.* 8, eabl5547.
- Teichert, M., Bolz, J., 2018. How senses work together: cross-modal interactions between primary sensory cortices. *Neural Plast.* 2018, 5380921.
- Thiele, A., Bellgrove, M.A., 2018. Neuromodulation of attention. *Neuron* 97, 769–785.
- Uludag, K., 2008. Transient and sustained BOLD responses to sustained visual stimulation. *Magn. Reson. Imaging* 26, 863–869.
- Van der Werf, Y.D., Witter, M.P., Groenewegen, H.J., 2002. The intralaminar and midline nuclei of the thalamus. Anatomical and functional evidence for participation in processes of arousal and awareness. *Brain Res. Brain Res. Rev.* 39, 107–140.
- Van Essen, D.C., Smith, S.M., Barch, D.M., Behrens, T.E., Yacoub, E., Ugurbil, K., 2013. The WU-Minn Human Connectome Project: an overview. *Neuroimage* 80, 62–79.
- Veldhuizen, M.G., Farruggia, M.C., Gao, X., Nakamura, Y., Green, B.G., Small, D.M., 2020. Identification of an amygdala thalamic circuit that acts as a Central gain mechanism in taste perceptions. *J. Neurosci.* 40, 5051–5062.
- Visscher, K.M., Miezin, F.M., Kelly, J.E., et al., 2003. Mixed blocked/event-related designs separate transient and sustained activity in fMRI. *Neuroimage* 19, 1694–1708.
- Wall, M.B., Walker, R., Smith, A.T., 2009. Functional imaging of the human superior colliculus: an optimised approach. *Neuroimage* 47, 1620–1627.
- Wang, L., Herman, J.P., Krauzlis, R.J., 2022. Neuronal modulation in the mouse superior colliculus during covert visual selective attention. *Sci. Rep.* 12, 2482.
- Williams, R.J., McMahon, K.L., Hocking, J., Reutens, D.C., 2014. Comparison of block and event-related experimental designs in diffusion-weighted functional MRI. *J. Magn. Reson. Imaging* 40, 367–375.
- Williams, R.J., Reutens, D.C., Hocking, J., 2016. Influence of BOLD contributions to diffusion fMRI activation of the visual cortex. *Front. Neurosci.* 10.
- Worsley, K.J., Friston, K.J., 1995. Analysis of Fmri Time-Series revisited - again. *Neuroimage* 2, 173–181.
- WU-Minn. HCP 1200 subjects data release reference manual. 2017. Accessed at: <https://www.humanconnectome.org>.
- Xiao, Y., Fonov, V., Chakravarty, M.M., et al., 2017. A dataset of multi-contrast population-averaged brain MRI atlases of a Parkinson's disease cohort. *Data Brief.* 12, 370–379.
- Xu, J., Galardi, M.M., Pok, B., et al., 2020. Thalamic stimulation improves postictal cortical arousal and behavior. *J. Neurosci.* 40, 7343–7354.
- Yanaka, H.T., Saito, D.N., Uchiyama, Y., Sadato, N., 2010. Neural substrates of phasic alertness: a functional magnetic resonance imaging study. *Neurosci. Res.* 68, 51–58.
- Yeon, J., Kim, J., Ryu, J., Park, J.Y., Chung, S.C., Kim, S.P., 2017. Human brain activity related to the tactile perception of stickiness. *Front. Hum. Neurosci.* 11, 8.